Enabling Situational Awareness in Millimeter Wave Massive MIMO Systems

Rico Mendrzik, *Student Member, IEEE*, Florian Meyer, *Member, IEEE*, Gerhard Bauch, *Fellow, IEEE*, and Moe Z. Win, *Fellow, IEEE*

***Abstract*—Situational awareness in wireless networks refers to the availability of position information on transmitters and receivers as well as information on their propagation environments to aid wireless communications. In millimeter wave massive multiple-input multiple-output communication systems, situational awareness can significantly improve the quality and robustness of communications. In this paper, we establish a model that describes the statistical dependencies between channel state information and the position, orientation, and clock offset of a user equipment along with the locations of features in the propagation environment. Based on this model, we introduce COMPAS (COncurrent Mapping, Positioning, And Synchronization); an inference engine that can provide accurate and reliable situational awareness in millimeter wave massive multiple-input multiple-output communication systems. Numerical results show that COMPAS is able to infer the positions of an unknown and time-varying number of features in the propagation environment and, at the same time, estimate the position, orientation, and clock offset of a user equipment.**

***Index Terms*—Millimeter wave, MIMO, positioning, synchronization, mapping.**

I. Introduction

LOCATION-AWARENESS [1]–[25] and knowledge of the propagation environment can enhance the performance of communication systems substantially [26]–[28]. Obtaining accurate and reliable information on the positions of user equipments (UEs) and their environments is a notoriously challenging problem in wireless communication systems. To address this challenge, approaches for multipath-assisted localization and mapping [29]–[34] in single antenna systems have been proposed recently. In particular, existing works are based on range measurements extracted from ultra-wideband (UWB) signals [29]–[31] and signals of opportunity (SOO) [32]–[34] provided by communication technologies such as long term evolution (LTE) and wireless fidelity (WiFi).

Millimeter wave (mmWave) massive multiple-input multiple-output (mMIMO) [35]–[37] will begin a new era of multipath-assisted localization due to the availability of precise angle-of-departure (AOD) and angle-of-arrival (AOA) information [38]–[40]. In addition to localization, mmWave mMIMO will make it possible to synchronize [41]–[43] UEs and map [44]–[46] their propagation environments. Localization and orientation estimation from angular measurements has been considered in [47]–[49]. Bayesian methods for static localization and mapping in mmWave mMIMO have been introduced in [50]–[52].

Enabling reliable and scalable localization and mapping in dynamic scenarios raises the following principle questions. Which mechanisms assure resilience to corrupted or missing measurements? What techniques render scalability in terms of the number of features in the map? Which practicability requirements (e.g., imprecise synchronization) must be addressed? The answers to these questions will guide the way towards situational awareness, which can aid mmWave mMIMO communication systems.

We promote situational awareness for future communication systems where information on the locations of UEs and knowledge of their propagation environments are determined. Situational awareness goes beyond the concept of location awareness since information on the propagation environment is explicitly considered. We expect that situational-aware communications will transform many facets of conventional communication systems and we believe that obtaining a map of the propagation environment can significantly improve the communication rate and reliability of future wireless systems. For instance, being aware of reflecting objects allows to establish side links that can increase transmission throughput, network capacity, and robustness. Fig. 1 depicts a selection of aspects where communications can benefit from situational awareness and vice versa. These aspects are not explicitly studied in this work but indicate relevant directions of future research.

The goal of this paper is to build the foundation for situational-aware communications by providing a powerful inference engine. Particularly, we consider the setting shown in Fig. 2 and propose COMPAS (COncurrent Mapping, Positioning, And Synchronization). COMPAS is based on a recently introduced framework for estimating an unknown number of objects in the

Manuscript received February 15, 2019; revised June 3, 2019 and July 10, 2019; accepted July 11, 2019. Date of publication August 15, 2019; date of current version September 20, 2019. This work was supported in part by the U.S. Department of Commerce, National Institute of Standards and Technology under Grant 70NANB17H17 and in part by the Austrian Science Fund under Grant J3886-N31. This paper was presented at the IEEE International Workshop on Signal Processing Advances in Wireless Communications, Cannes, France, July 2019. The guest editor coordinating the review of this paper and approving it for publication was Dr. Erik G. Larsson. *(Corresponding author: Rico Mendrzik.)*

R. Mendrzik is with the INT, Hamburg University of Technology, 21073 Hamburg, Germany, and also with the Wireless Information and Network Sciences Laboratory, Massachusetts Institute of Technology, Cambridge, MA 02139 USA (e-mail: rico.mendrzik@tuhh.de).

F. Meyer is with the Wireless Information and Network Sciences Laboratory, Massachusetts Institute of Technology, Cambridge, MA 02139 USA (e-mail: fmeyer@mit.edu).

G. Bauch is with the INT, Hamburg University of Technology, 21073 Hamburg, Germany (e-mail: bauch@tuhh.de).

M. Z. Win is with the Laboratory for Information and Decision Systems, Massachusetts Institute of Technology, Cambridge, MA 02139 USA (e-mail: win@mit.edu).

Digital Object Identifier 10.1109/JSTSP.2019.2933142

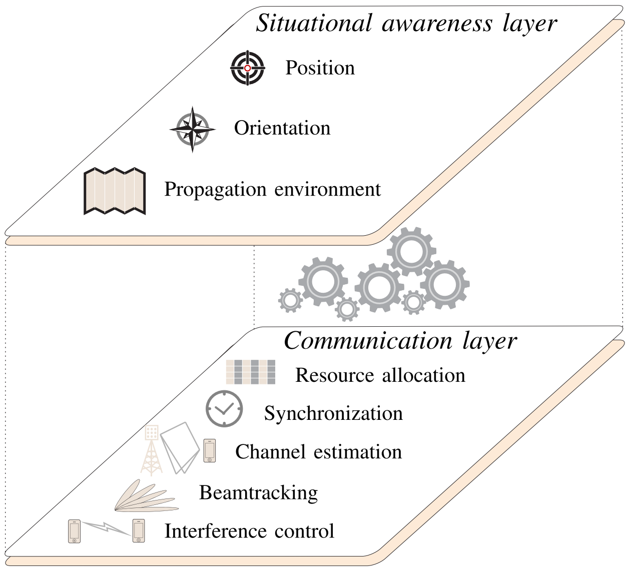

Fig. 1. Interplay of situational awareness and communications. The situational awareness layer determines information on the positions and orientations of UEs and on their propagation environments to aid the communication layer. We propose a method for achieving situational awareness in this article.

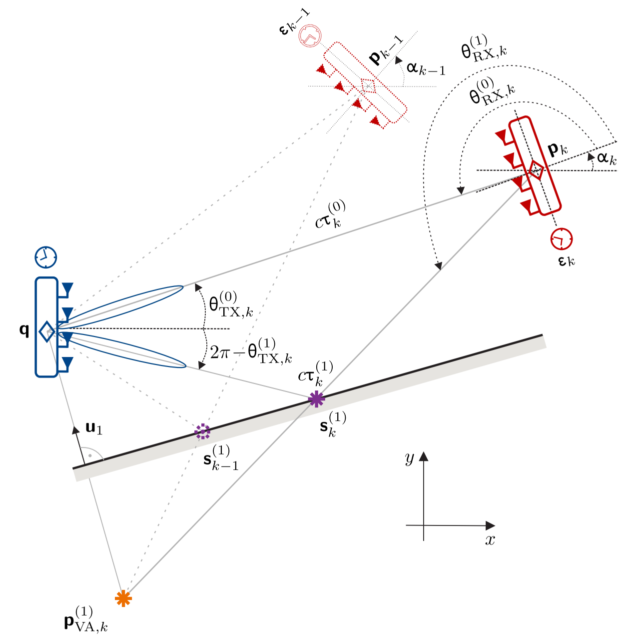

Fig. 2. Situational awareness provided by mmWave mMIMO communications. The UE (red array) changes its position p_k, orientation α_k, and clock offset ϵ_k between any two time steps $k-1$ and k. At every time step k, it receives the signals from the BS (blue array) based on which it extracts the AOAs $\theta^{(j)}_{\mathrm{RX},k}$, AODs $\theta^{(j)}_{\mathrm{TX},k}$, and delay $\tau^{(j)}_k$ of every received path j. NLOS paths are generated by reflecting surfaces that can be represented by VAs, e.g., $\mathsf{p}^{(1)}_{\mathrm{VA},k}$. While the point of reflection $\mathsf{s}^{(1)}_k$ moves as the position of the UE changes, the VA remains in the same location.

presence of measurement origin uncertainty [53]. It enables joint tracking of the position, orientation, and clock offset of a UE as well as the generation of a map of reflecting surfaces in the propagation environment. The key contributions of this paper are as follows.

- We develop a stochastic model for the relationship of information on the UE state (position, orientation, and clock offset) and information on the propagation environment available in mmWave mMIMO systems.
- We derive COMPAS, a robust and scalable inference engine that infers the states of a UE along with the positions of reflecting surfaces in its propagation environment.
- We demonstrate via numerical examples that COMPAS provides accurate and robust information regarding the UE states and its propagation environment.

In contrast to classical simultaneous localization and mapping (SLAM), we estimate the clock offset in addition to UE position and orientation. On the other hand, our methodology does not consider loop-closure, which is a fundamental element in SLAM [46].

The remaining sections are organized as follows. Section II introduces the state-space model, channel estimation based on angular models, the geometric relationship between the channel parameters and position-related parameters, and the measurement model. The section is concluded with the definition of the inference problem. The stochastic model derived in this paper is presented in Section III by providing an intuition, a rigorous mathematical description, and a graphical representation of the model. Section IV presents COMPAS; our inference engine for the model developed in Section III. A numerical analysis of COMPAS is conducted in Section V, and Section VI makes concluding remarks.

Notation: Random variables are displayed in sans serif, upright fonts; their realizations in serif, italic fonts. Vectors and matrices are denoted by bold lowercase and uppercase letters, respectively. For example, a random variable and its realization are denoted by x and x; a random vector and its realization are denoted by $\boldsymbol{\mathsf{x}}$ and $\boldsymbol{x}$. Sets are denoted by calligraphic font, e.g., $\mathcal{X}$. An estimate of a parameter is denoted with the superscript hat, e.g., $\hat{x}$. Furthermore, $\|\boldsymbol{x}\|$, $\boldsymbol{x}^{\mathrm{T}}$, and $\boldsymbol{x}^{\mathrm{H}}$ denote the Euclidean norm, the transpose of vector $\boldsymbol{x}$, and the conjugate transpose of vector $\boldsymbol{x}$, respectively; $\propto$ indicates equality up to a normalization factor; $f(\boldsymbol{x})$ denotes the probability density function (PDF) of random vector $\boldsymbol{\mathsf{x}}$ (this is a short notation for $f_{\boldsymbol{\mathsf{x}}}(\boldsymbol{x})$); $f(\boldsymbol{x}|\boldsymbol{y})$ denotes the conditional PDF of random vector $\boldsymbol{\mathsf{x}}$ conditioned on random vector $\boldsymbol{\mathsf{y}}$; $|\mathcal{S}|$ denotes the cardinality of set $\mathcal{S}$; $\boldsymbol{I}_n$ denotes the $n \times n$ identity matrix. The indicator function is denoted by $\mathbb{I}(\cdot)$.

II. Problem Formulation

This section describes the fundamental models that we consider and defines the inference problem.

A. State-Space Model

We consider a mmWave mMIMO communication system with a static base station (BS) and a UE. The BS and the UE are equipped with large antenna arrays of arbitrary geometry. Let φ_k and α_k denote the orientation of the array of the BS and UE at time k, respectively. The locations of the BS and UE are given by the centroids of their arrays and they are denoted by $\boldsymbol{\mathsf{q}}_k \triangleq [\mathsf{q}_{\mathrm{x},k}\; \mathsf{q}_{\mathrm{y},k}]^{\mathrm{T}}$ and $\boldsymbol{\mathsf{p}}_k \triangleq [\mathsf{p}_{\mathrm{x},k}\; \mathsf{p}_{\mathrm{y},k}]^{\mathrm{T}}$, respectively. We consider a two-dimensional (2D) model for the sake of simplicity. An extension to three dimensions is possible in a straightforward manner. It it assumed that the BS is static, and its position and orientation are known, i.e., $\boldsymbol{\mathsf{q}}_k = \boldsymbol{q}$ and $\varphi_k = \varphi$.

Without loss of generality we set $\varphi = 0$. The clocks of the BS and UE are not accurately synchronized and their clock offset is described by ϵ_k. The propagation environment consists of a time-varying number of reflecting surfaces with indices $l \in \mathcal{I}_k$. We describe a reflecting surface $l \in \mathcal{I}_k$ by a normal vector $\mathbf{u}_l$ and an arbitrary point $\mathbf{v}_l$ on the reflecting surface. These surfaces are represented by static virtual anchors (VAs)[1] which are located at mirror images of the BS position at the reflecting surfaces. Note that the positions of VAs are assumed to be static but their presence can change over time, i.e., new reflectors can appear in the environment and existing reflectors can disappears. The position $\mathbf{p}_{\mathrm{VA},k}^{(l)} = [\mathrm{p}_{\mathrm{VA,x},k}^{(l)} \ \mathrm{p}_{\mathrm{VA,y},k}^{(l)}]^{\mathrm{T}}$ of the lth VA is given by

$$\boldsymbol{p}_{\mathrm{VA},k}^{(l)} = \left(\boldsymbol{I}_2 - 2\boldsymbol{u}_l\boldsymbol{v}_l^{\mathrm{T}}\right)\boldsymbol{q} + 2\boldsymbol{v}_l^{\mathrm{T}}\boldsymbol{u}_l\boldsymbol{u}_l. \tag{1}$$

Neither the number $|\mathcal{I}_k|$ of reflecting surfaces nor the positions $\mathbf{p}_{\mathrm{VA},k}^{(l)}, l \in \mathcal{I}_k$ of the corresponding virtual anchors are known. If VA l existed at time $k-1$, it also exists at time k with probability $P_{\mathrm{s}}(\boldsymbol{p}_{\mathrm{VA},k-1}^{(l)})$. The arrival or birth of new features is modeled by a Poisson point process with intensity function $\lambda_{\mathrm{b}}(\breve{\boldsymbol{p}}_{\mathrm{VA},k}) \triangleq m_{\mathrm{b}} f_{\mathrm{b}}(\breve{\boldsymbol{p}}_{\mathrm{VA},k})$ with $\breve{\mathbf{p}}_{\mathrm{VA},k} \in \mathbb{R}^2$.

UE position $\mathbf{p}_k$, orientation α_k, clock offset ϵ_k, and VA positions $\mathbf{p}_{\mathrm{VA},k}^{(l)}, l \in \mathcal{I}_k$ are assumed to evolve independently over time. Thus, their joint state-transition function is given by

$$\begin{aligned} &f(\boldsymbol{p}_{\mathrm{VA},k}, \boldsymbol{p}_k, \alpha_k, \epsilon_k | \boldsymbol{p}_{\mathrm{VA},k-1}, \boldsymbol{p}_{k-1}, \alpha_{k-1}, \epsilon_{k-1}) \\ &\quad = f(\boldsymbol{p}_k|\boldsymbol{p}_{k-1}) f(\alpha_k|\alpha_{k-1}) f(\epsilon_k|\epsilon_{k-1}) \prod_{l\in\mathcal{I}_k} f(\boldsymbol{p}_{\mathrm{VA},k}^{(l)}|\boldsymbol{p}_{\mathrm{VA},k-1}^{(l)}) \end{aligned} \tag{2}$$

where $\mathbf{p}_{\mathrm{VA},k} \triangleq [\mathbf{p}_{\mathrm{VA},k}^{(1)\mathrm{T}} \, \mathbf{p}_{\mathrm{VA},k}^{(2)\mathrm{T}} \cdots \mathbf{p}_{\mathrm{VA},k}^{(|\mathcal{I}_k|)\mathrm{T}}]^{\mathrm{T}}$ and $f(\boldsymbol{p}_{\mathrm{VA},k}^{(l)}| \boldsymbol{p}_{\mathrm{VA},k-1}^{(l)}) = f_{\mathrm{b}}(\boldsymbol{p}_{\mathrm{VA},k}^{(l)})$ if VA $l \in \mathcal{I}_k$ was born at time k and $f(\boldsymbol{p}_{\mathrm{VA},k}^{(l)}|\boldsymbol{p}_{\mathrm{VA},k-1}^{(l)}) = \delta(\boldsymbol{p}_{\mathrm{VA},k}^{(l)} - \boldsymbol{p}_{\mathrm{VA},k-1}^{(l)})$ if VA $l \in \mathcal{I}_k$ already existed at time $k-1$. For $k=1$, we define $f(\boldsymbol{p}_{\mathrm{VA},1}, \boldsymbol{p}_1, \alpha_1, \epsilon_1 | \boldsymbol{p}_{\mathrm{VA},0}, \boldsymbol{p}_0, \alpha_0, \epsilon_0) \triangleq f(\boldsymbol{p}_1) f(\alpha_1) f(\epsilon_1) \prod_{l\in\mathcal{I}_1} f_{\mathrm{b}}(\boldsymbol{p}_{\mathrm{VA},1}^{(l)})$, where $f(\boldsymbol{p}_1)$, $f(\alpha_1)$, and $f(\epsilon_1)$ denote the prior PDFs of the UE position $\mathbf{p}_1$, orientation α_1, and clock offset ϵ_1 at time $k=1$. These prior PDFs are assumed statistically independent.

B. Channel Estimation Based on Angular Models

The BS periodically transmits pilot signals $\tilde{\boldsymbol{s}}_k(t) = [\tilde{s}_{k,1}(t) \ \tilde{s}_{k,2}(t) \cdots \tilde{s}_{k,N_{\mathrm{B}}}(t)]^{\mathrm{T}}$ to the UE using N_{B} beams. These signals are precoded according to $\boldsymbol{s}_k(t) = \boldsymbol{F}_k\tilde{\boldsymbol{s}}_k(t)$, where $\boldsymbol{F}_k = [\boldsymbol{f}_{k,1} \ \boldsymbol{f}_{k,2} \cdots \boldsymbol{f}_{k,N_{\mathrm{B}}}]$ contains N_{B} beamforming vectors $\boldsymbol{f}_{k,i}$. The precoded signal $\boldsymbol{s}_k(t)$ is transmitted over a channel with J_k paths. The AOAs, AODs, and delay of the j^{th} path are denoted by $\theta_{\mathrm{RX},k}^{(j)}$, $\theta_{\mathrm{TX},k}^{(j)}$, and $\tau_k^{(j)}$, respectively. We collect these quantities in the following vectors $\boldsymbol{\theta}_{\mathrm{RX},k} = [\theta_{\mathrm{RX},k}^{(0)}\theta_{\mathrm{RX},k}^{(1)} \cdots \theta_{\mathrm{RX},k}^{(J_k)}]^{\mathrm{T}}$, $\boldsymbol{\theta}_{\mathrm{TX},k} = [\theta_{\mathrm{TX},k}^{(0)}\theta_{\mathrm{TX},k}^{(1)} \cdots \theta_{\mathrm{TX},k}^{(J_k)}]^{\mathrm{T}}$, and $\boldsymbol{\tau}_k = [\tau_k^{(0)}\tau_k^{(1)} \cdots \tau_k^{(J_k)}]^{\mathrm{T}}$. The impulse response of the channel in the equivalent baseband is given by [37] $\boldsymbol{H}_k(t) = \sum_{j=0}^{J_k} h_k^{(j)} \boldsymbol{a}_{\mathrm{RX}}(\theta_{\mathrm{RX},k}^{(j)}) \boldsymbol{a}_{\mathrm{TX}}^{\mathrm{H}}(\theta_{\mathrm{TX},k}^{(j)}) \delta(t - \tau_k^{(j)})$,

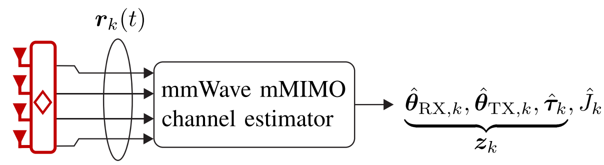

Fig. 3. Parameter estimation of the mmWave mMIMO channel. The AOA $\hat{\boldsymbol{\theta}}_{\mathrm{RX},k}$, AOD $\hat{\boldsymbol{\theta}}_{\mathrm{TX},k}$, and delay $\hat{\boldsymbol{\tau}}_k$ estimates and the detected number $\hat{J}_k$ of paths are obtained by feeding the received signal $\boldsymbol{r}_k(t)$ into an angle-based channel estimator.

where $h_k^{(j)}$ is the complex channel coefficient of the j^{th} path, while $\boldsymbol{a}_{\mathrm{RX}}$ and $\boldsymbol{a}_{\mathrm{TX}}$ denote the receiver's and transmitter's array response vector, respectively. It is assumed that non-line-of-sight (NLOS) components originate from single-bounce reflections due to the high path loss and the directionality of the arrays [54]. The UE receives the noisy downlink signal $\boldsymbol{r}_k(t)$ at every time step k, i.e., $\boldsymbol{r}_k(t) = \sum_{j=0}^{J_k} h_k^{(j)} \boldsymbol{a}_{\mathrm{RX}}(\theta_{\mathrm{RX},k}^{(j)}) \boldsymbol{a}_{\mathrm{TX}}^{\mathrm{H}}(\theta_{\mathrm{TX},k}^{(j)}) \boldsymbol{s}_k(t - \tau_k^{(j)}) + \boldsymbol{n}_k(t)$, where $\boldsymbol{n}_k(t)$ is the additive noise vector. This signal is fed into an angle-based channel estimator that computes estimates of the AOAs, AODs, delays, and the number of paths as depicted in Fig. 3. Such channel estimators for mmWave mMIMO have been presented in [40], [55]–[57]. We index the line-of-sight (LOS) path with $j=0$ and assume that the LOS path can be identified reliably, e.g., based on the significantly higher power level compared to NLOS paths [58]. Moreover, we assume coarse synchronization on symbol level as required for channel estimation. However, the precise clock offset ϵ_k, required for accurately determining the path lengths $c\tau_k^{(j)}$, $j \in \{0, 1, \ldots, J_k\}$ is still assumed unknown. The estimates $\hat{\theta}_{\mathrm{RX},k}^{(j)}$, $\hat{\theta}_{\mathrm{TX},k}^{(j)}$, and $\hat{\tau}_k^{(j)}$ corresponding to the j^{th} path are subject to estimation errors which are assumed statistically independent. Furthermore, estimation errors are also assumed statistically independent across different paths.

C. From Channel Parameters to Position-Related Parameters

The relationships between UE states, VAs and reflection point positions, and channel parameters are given by the following list of equations

$$\tau_k^{(0)} = \frac{||\boldsymbol{q} - \boldsymbol{p}_k||}{c} + \epsilon_k \tag{3a}$$

$$\begin{aligned} \tau_k^{(j)} &= \frac{||\boldsymbol{q} - \boldsymbol{s}_k^{(j)}|| + ||\boldsymbol{s}_k^{(j)} - \boldsymbol{p}_k||}{c} + \epsilon_k \\ &= \frac{||\boldsymbol{p}_{\mathrm{VA},k}^{(j)} - \boldsymbol{p}_k||}{c} + \epsilon_k \end{aligned} \tag{3b}$$

$$\theta_{\mathrm{TX},k}^{(0)} = \mathrm{atan2}\left(p_{\mathrm{y},k} - q_{\mathrm{y}}, p_{\mathrm{x},k} - q_{\mathrm{x}}\right) \tag{3c}$$

$$\theta_{\mathrm{TX},k}^{(j)} = \mathrm{atan2}\left(s_{\mathrm{y},k}^{(j)} - q_{\mathrm{y}}, s_{\mathrm{x},k}^{(j)} - q_{\mathrm{x}}\right) \tag{3d}$$

$$\theta_{\mathrm{RX},k}^{(0)} = \mathrm{atan2}\left(q_{\mathrm{y}} - p_{\mathrm{y},k}, q_{\mathrm{x}} - p_{\mathrm{x},k}\right) - \alpha_k \tag{3e}$$

$$\begin{aligned} \theta_{\mathrm{RX},k}^{(j)} &= \mathrm{atan2}\left(s_{\mathrm{y},k}^{(j)} - p_{\mathrm{y},k}, s_{\mathrm{x},k}^{(j)} - p_{\mathrm{x},k}\right) - \alpha_k \\ &= \mathrm{atan2}\left(p_{\mathrm{VA,y},k}^{(j)} - p_{\mathrm{y},k}, p_{\mathrm{VA,x},k}^{(j)} - p_{\mathrm{x},k}\right) - \alpha_k \end{aligned} \tag{3f}$$

[1]We will use the terms VAs, features, and reflecting surfaces interchangeably throughout this paper.

where $j \in \{1, 2, \ldots, J_k\}$, c is the speed of light, atan2 denotes the four-quadrant inverse tangent, and the point of reflection $\boldsymbol{s}_k^{(j)} = [s_{\mathrm{x},k}^{(j)}\ s_{\mathrm{y},k}^{(j)}]^{\mathrm{T}}$ is given as

$$\boldsymbol{s}_k^{(j)} = \boldsymbol{p}_{\mathrm{VA},k}^{(j)} + \frac{(\boldsymbol{f}_j - \boldsymbol{p}_{\mathrm{VA},k}^{(j)})^{\mathrm{T}} \boldsymbol{u}_j}{(\boldsymbol{p}_k - \boldsymbol{p}_{\mathrm{VA},k}^{(j)})^{\mathrm{T}} \boldsymbol{u}_j} (\boldsymbol{p}_k - \boldsymbol{p}_{\mathrm{VA},k}^{(j)}) \tag{4}$$

with $\boldsymbol{f}_j = (\boldsymbol{q} + \boldsymbol{p}_{\mathrm{VA},k}^{(j)})/2$. Note that the mathematical relationship between the UE, VA, and its reflection point described by (4) is required to connect the AOD of an NLOS path with the positions of the VA and UE (cf. Fig. 2 for a geometric interpretation).

D. Measurement Model

We consider the estimates provided by the angle-based channel estimator as the observations or measurements in the underlying inference problem. Thus, the j^{th} measurement at time k is denoted by $\boldsymbol{z}_k^{(j)} \triangleq [z_{\theta_{\mathrm{RX}},k}^{(j)}\ z_{\theta_{\mathrm{TX}},k}^{(j)}\ z_{\tau,k}^{(j)}]^{\mathrm{T}}$ with entries $z_{\theta_{\mathrm{RX}},k}^{(j)} \triangleq \hat{\theta}_{\mathrm{RX},k}^{(j)}$, $z_{\theta_{\mathrm{TX}},k}^{(j)} \triangleq \hat{\theta}_{\mathrm{TX},k}^{(j)}$, and $z_{\tau,k}^{(j)} \triangleq \hat{\tau}_k^{(j)}$. Furthermore, we introduce the number of measurements $M_k \triangleq \hat{J}_k$ as well as the joint measurement vector $\boldsymbol{z}_k \triangleq [\boldsymbol{z}_k^{(0)\mathrm{T}}\ \boldsymbol{z}_k^{(1)\mathrm{T}} \cdots \boldsymbol{z}_k^{(M_k)\mathrm{T}}]^{\mathrm{T}}$. The joint likelihoods of the NLOS and LOS measurements are given by $f(\boldsymbol{z}_k^{(j)} | \boldsymbol{p}_{\mathrm{VA},k}^{(j)}, \boldsymbol{p}_k, \epsilon_k, \alpha_k) = f(z_{\tau,k}^{(j)} | \boldsymbol{p}_{\mathrm{VA},k}^{(j)}, \boldsymbol{p}_k, \epsilon_k) f(z_{\theta_{\mathrm{RX}},k}^{(j)} | \boldsymbol{p}_{\mathrm{VA},k}^{(j)}, \boldsymbol{p}_k, \alpha_k) f(z_{\theta_{\mathrm{TX}},k}^{(j)} | \boldsymbol{p}_{\mathrm{VA},k}^{(j)}, \mathbf{p}_k)$ and

$$\begin{aligned} &f\big(\boldsymbol{z}_k^{(0)} | \boldsymbol{p}_k, \epsilon_k, \alpha_k\big) \\ &\quad = f\big(z_{\tau,k}^{(0)} | \boldsymbol{p}_k, \epsilon_k\big) f\big(z_{\theta_{\mathrm{RX}},k}^{(0)} | \boldsymbol{p}_k, \alpha_k\big) f\big(z_{\theta_{\mathrm{TX}},k}^{(0)} | \boldsymbol{p}_k\big). \end{aligned} \tag{5}$$

The individual NLOS likelihood functions $f(z_{\tau,k}^{(j)} | \boldsymbol{p}_{\mathrm{VA},k}^{(j)}, \boldsymbol{p}_k, \epsilon_k)$, $f(z_{\theta_{\mathrm{RX}},k}^{(j)} | \boldsymbol{p}_{\mathrm{VA},k}^{(j)}, \boldsymbol{p}_k, \alpha_k)$, and $f(z_{\theta_{\mathrm{TX}},k}^{(j)} | \boldsymbol{p}_{\mathrm{VA},k}^{(j)}, \mathbf{p}_k)$ can directly be obtained from the estimation error statistics and (3b), (3d), and (3f), respectively. Similarly LOS likelihood functions are obtained from estimation error statistics and (3a), (3c), and (3e).

Note that the estimated number $\hat{J}_k$ of paths generated by the angle-based channel estimator does not necessarily match the number of channel paths caused by first order reflections. Errors occur due to missed detections and false alarms (clutter) [59]. Missed detections describe the cases in which existing first order paths are not observed by the channel estimator. False alarms or clutter are measurements that cannot be explained as first order reflections.[2] We assume that the number of clutter measurements is Poisson distributed with mean m_{c}. Clutter measurements are assumed independent and identically distributed (iid) and statistically independent of measurements related to actual paths. Hence their distributions are given by $f_{\mathrm{c}}(\boldsymbol{z}_k^{(j)}) = f_{\mathrm{c}}(z_{\tau,k}^{(j)}) f_{\mathrm{c}}(z_{\theta_{\mathrm{RX}},k}^{(j)}) f_{\mathrm{c}}(z_{\theta_{\mathrm{TX}},k}^{(j)})$. The probability that the l^{th} existing feature $\mathbf{p}_{\mathrm{VA},k}^{(l)}$ is detected, i.e., generates a measurement, is generally a function of $\mathbf{p}_{\mathrm{VA},k}^{(l)}$, $\mathbf{p}_k$, and $\boldsymbol{\alpha}_k$. This function is denoted by $P_{\mathrm{d}}(\boldsymbol{p}_{\mathrm{VA},k}^{(l)}, \boldsymbol{p}_k, \alpha_k)$ and assumed to be known.[3]

E. Inference Problem

The aim of this paper is to solve the following problem. Given a sequence of measurement $\boldsymbol{z}_{1:K} \triangleq [\boldsymbol{z}_1^{\mathrm{T}}\ \boldsymbol{z}_2^{\mathrm{T}} \cdots \boldsymbol{z}_K^{\mathrm{T}}]^{\mathrm{T}}$ derived from the mmWave mMIMO downlink signals $\boldsymbol{r}_{1:K}(t) \triangleq [\boldsymbol{r}_1^{\mathrm{T}}(t)\ \boldsymbol{r}_2^{\mathrm{T}}(t) \cdots \boldsymbol{r}_K^{\mathrm{T}}(t)]^{\mathrm{T}}$, the UE attempts to estimate its positions $\mathbf{p}_k$, orientations $\boldsymbol{\alpha}_k$, and clock offsets $\boldsymbol{\varepsilon}_k$ at all times $k = 1, 2, \ldots, K$ in a sequential manner. At the same time, the UE seeks to infer the number $|\mathcal{I}_k|$ and positions $\mathbf{p}_{\mathrm{VA},k}^{(l)}, \forall l \in \mathcal{I}_k$ of all VAs. In other words, the UE tries to estimate its own states while building a map of reflecting surfaces in its propagation environment.

III. Stochastic Problem Formulation

In this section, we will present the stochastic model used in COMPAS by providing an intuitive explanation and a rigorous mathematical description that can be represented by a factor graph. We build upon the approaches in [30], [53], [61] in order to derive our stochastic model. However, our approach differs from [30], [53], [61] in that we consider separated UE states, i.e., the position $\mathbf{p}_k$, orientation $\boldsymbol{\alpha}_k$, and clock offset $\boldsymbol{\varepsilon}_k$ of the UE are split into independent states. Our model extends beyond previous works since we also incorporate angular measurements (AODs and AOAs) and exploit the fact that the joint likelihood function can be factorized in individual components for delay, AOD, and AOA.

A. Overview of the Stochastic Model

The number of propagation paths is time-varying and unknown, the UE cannot observe the entire propagation environment at once, and the channel estimator may not detect existing paths (missed detection) or generate clutter measurements (false alarms). For these reasons, the UE must be able to accommodate an unknown and time-varying number of features in its stochastic model of the environment. At time k, we distinguish between the following two types of actually existing features:

- *newly detected features*, which exist at time k and have generated a measurement for the first time at time k;
- *previously detected features*, which exist at time k and have generated a measurement at a previous time $k' < k$.

The numbers of newly detected features and previously detected features are unknown. To account for this fact in our stochastic model, we use the notion of potential features (PFs) [44], [53], [61]. The l^{th} PF is mathematically described by $\mathbf{x}_k^{(l)} \triangleq [\mathbf{p}_{\mathrm{VA},k}^{(l)\mathrm{T}}\ \ \mathsf{r}_k^{(l)}]^{\mathrm{T}}$, where $\mathsf{r}_k^{(l)} \in \{0, 1\}$ is a binary variable that indicates the existence of a PF. In particular, if $\mathsf{r}_k^{(l)} = 1$, then PF l corresponds to an actual feature in the propagation environment. It will be discussed in Section IV-A that the representation by means of PFs also allows to assign an existence probability to each PF.

The key idea of our model is elaborated in the following. At time k, we add a new PF $\overline{\mathbf{x}}_k^{(j)} \triangleq [\overline{\mathbf{p}}_{\mathrm{VA},k}^{(j)\mathrm{T}}\ \overline{\mathsf{r}}_k^{(j)}]^{\mathrm{T}}$, $j \in \mathcal{M}_k$ to the state space for every NLOS measurement $\boldsymbol{z}_k^{(j)}$, $j \in \mathcal{M}_k$, where

[2] In our model, measurements erroneously extracted by the channel estimator as well as measurements related to higher order reflections are considered as clutter.

[3] Following [60], the detection probability P_{d} can also be modeled as a random variable and inferred online.

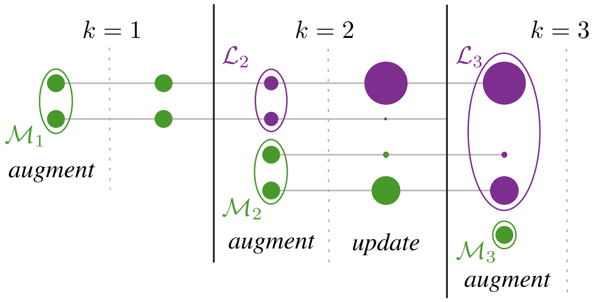

Fig. 4. Stochastic model with dynamic state-space augmentation. Each measurement generates a new PF (green circles) in the state space. The states of these PFs (VA positions and binary existence indicators) are updated based on the measurements of the current time instance. The existence probability is encoded by the size of the circles. The union of the sets of new $\mathcal{M}_k$ and legacy $\mathcal{L}_k$ (magenta circles) PFs becomes the set $\mathcal{L}_{k+1}$ of legacy PFs in the next time step $k+1$. For tractability, features whose existence probability is too small will be removed and hence not be propagated forward in the time.

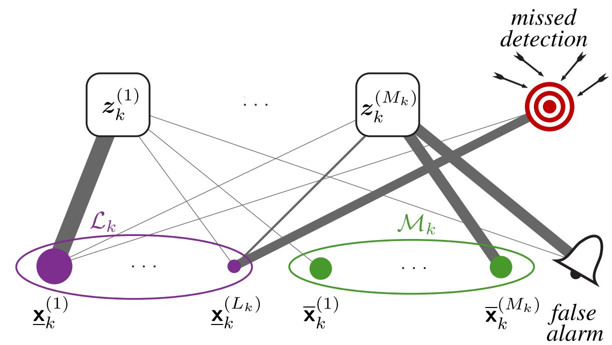

Fig. 5. Probabilistic data association. Measurements are associated with legacy $\underline{\mathbf{x}}_k^{(l)}, l \in \mathcal{L}_k$ and new $\overline{\mathbf{x}}_k^{(j)}, j \in \mathcal{M}_k$ PFs in a probabilistic manner. The thickness of the lines indicates the association probabilities. Examples: The first measurement $\boldsymbol{z}_k^{(1)}$ is generated by the legacy PF $\underline{\mathbf{x}}_k^{(1)}$ with high probability, while the probability that the new PF $\overline{\mathbf{x}}_k^{(1)}$ generated the first measurement is small due to the presence of the legacy PF $\underline{\mathbf{x}}_k^{(1)}$. In contrast, none of the legacy PFs $\underline{\mathbf{x}}_k^{(l)} \in \mathcal{L}_k$ reduces the association probability of the new PF $\overline{\mathbf{x}}_k^{(M_k)}$ with measurement $\boldsymbol{z}_k^{(M_k)}$ considerably, rendering its association likely. Since the new PF $\overline{\mathbf{x}}_k^{(M_k)}$ is observed for the first time, the probability that $\boldsymbol{z}_k^{(M_K)}$ is a false alarms is the same as the association probability with new PF $\overline{\mathbf{x}}_k^{(M_k)}$. Also, it is relatively likely that the legacy PF $\underline{\mathbf{x}}_k^{(L_k)}$ did not produce a measurement (missed detection).

$\mathcal{M}_k \triangleq \{1,2,\ldots,M_k\}$ is the index set of NLOS measurements. New PFs $\overline{\mathbf{x}}_k^{(j)}$ are introduced in addition to the legacy PFs $\underline{\mathbf{x}}_k^{(l)} \triangleq [\underline{\mathbf{p}}_{\mathrm{VA},k}^{(l)\mathrm{T}}\ \underline{\mathrm{r}}_k^{(l)}]^{\mathrm{T}}$, $l \in \mathcal{L}_k \triangleq \{1,2,\ldots,L_k\}$ that have been introduced at previous time steps (see Fig. 4). At time k, new $\overline{\mathbf{x}}_k^{(j)}$ and legacy $\underline{\mathbf{x}}_k^{(l)}$ PFs[4] are combined and represent the legacy PFs at $k+1$.

The overall procedure enables a *dynamic state-space augmentation* at each time instance. Before advancing to the next time instance, the states of all PFs must be updated. During the *state-space update*, the probabilities of existence and the distributions of the positions of all PFs in the state space are recalculated (see Fig. 4). This update step requires data association, where measurements are associated with PFs. An example of the probabilistic data association procedure considered in this paper is depicted in Fig. 5. Intuitively, the probabilistic data association procedure works as follows. The probabilities of all association hypotheses of PFs and measurements are evaluated. If a PF state explains a measurement well, the association probability will be high (indicated by thick gray lines in Fig. 5). The PF states are updated by considering all possible association hypotheses. After the update, the posterior probabilities of existence and the posterior distributions of the positions of PFs are available.

In our model, we add a PF for every observed NLOS measurement triplet. If an actual feature generates consistent measurements over time, multiple PFs will be generated that all represent the same actual feature. However, during data association, these PFs compete for the one measurement generated by the actual feature. Among these PFs, the PF that was added first, will typically have a high association probability to the respective measurement, while the other PFs will have low association probabilities. In turn, in the update step, the existence probabilities of the first PF related to the actual feature will be increased and the existence probabilities of the other PFs will be reduced. To prevent rapid growth of the state space, a sub-optimum *pruning* step is performed where PFs whose posterior existence probabilities drop below a certain threshold are removed from the state space. This step keeps the size of our stochastic model tractable for inference. Only those PFs that have not been removed by the pruning step are propagated forward to the next time step. After state-space augmentation, state-space update and pruning, an index mapping is performed such that $\mathcal{L}_{k+1} \triangleq \{1,2,\ldots,L_{k+1}\}$.

B. Mathematical Description of the Stochastic Model

In the following section, we describe the stochastic model mathematically. This model is embodied by the joint posterior distribution of the states of the UE, the PF states that model the propagation environment, and the associations variables that describe measurement-to-feature associations conditioned on all performed measurements. Before the final model will be presented, the state-transition model involving PFs and associations of measurements with PFs will be discussed. For the convenience of the reader, the important notation is summarized in Table I at the top of the next page.

1) PF States and the State-Transition Model: We model the existence/nonexistence of the l^{th} PF by a binary random variable $\mathrm{r}_k^{(l)} \in \{0,1\}$, i.e., PF l exists at time k if and only if $\mathrm{r}_k^{(l)} = 1$. The states $\mathbf{p}_{\mathrm{VA},k}^{(l)}$ of non-existing PFs are obviously not relevant but need to be considered formally also if $\mathrm{r}_k^{(l)} = 0$. Following [44], [53], [61], all PDFs defined for PF states, $f(\boldsymbol{x}_k^{(l)}) = f(\boldsymbol{p}_{\mathrm{VA},k}^{(l)}, r_k^{(l)})$, have the property that

$$f\big(\boldsymbol{p}_{\mathrm{VA},k}^{(l)}, 0\big) = P_k^{(l)} f_{\mathrm{D}}\big(\boldsymbol{p}_{\mathrm{VA},k}^{(l)}\big) \tag{6}$$

where $P_k^{(l)} \in [0,1]$ is the probability of non-existence and $f_{\mathrm{D}}(\boldsymbol{p}_{\mathrm{VA},k}^{(l)})$ is an arbitrary "dummy PDF". Newly detected features at every time step k are modeled by a Poisson point process with intensity function $\lambda_{\mathrm{n},k}(\breve{\boldsymbol{p}}_{\mathrm{VA},k})$, which depends

[4]Depending on the context, the symbols $\mathbf{x}_k^{(l)}$, $\mathbf{p}_{\mathrm{VA},k}^{(l)}$ and $\mathrm{r}_k^{(l)}$ denote the respective states of either a new or a legacy PF.

TABLE I
NOTATIONS OF IMPORTANT QUANTITIES

Notation	Definition	Notation	Definition
p_k	Position of the UE at time k	$\boldsymbol{z}_k$	Vector of NLOS measurement triplets at time k
α_k	Orientation of the UE at time k	$\mathcal{L}_k$	Index set of legacy PFs at time k
ϵ_k	Clock offset of the UE at time k	$\mathcal{M}_k$	Index set of new PFs at time k
$\underline{\mathsf{x}}_k^{(l)}$	State of the l^{th} legacy PF at time k	a_k	Feature-oriented data association (DA) vector at time k
$\underline{\mathsf{p}}_{\mathrm{VA},k}^{(l)}$	Position of the l^{th} legacy PF at time k	b_k	Measurement-oriented data association vector at time k
$\underline{\mathsf{r}}_k^{(l)}$	Existence probability of the l^{th} legacy PF at time k	$z_{\tau,k}^{(j)}$	Delay estimate of the j^{th} path at time k
$\overline{\mathsf{x}}_k^{(j)}$	State of the j^{th} new PF at time k	$z_{\theta_{\mathrm{RX}},k}^{(j)}$	AOA estimate of the j^{th} path at time k
$\overline{\mathsf{p}}_{\mathrm{VA},k}^{(j)}$	Position of the j^{th} new PF at time k	$z_{\theta_{\mathrm{TX}},k}^{(j)}$	AOD estimate of the j^{th} path at time k
$\overline{\mathsf{r}}_k^{(j)}$	Existence probability of the j^{th} new PF at time k	K	Number of time steps

on the birth intensity $\lambda_{\mathrm{b}}(\breve{\boldsymbol{p}}_{\mathrm{VA},k})$ and detection probability $P_{\mathrm{d}}(\breve{\boldsymbol{p}}_{\mathrm{VA},k}, \mathbf{p}_k, \alpha_k)$ (see [53] for details).

PF states x_k, position p_k, orientation α_k, and clock offset ϵ_k evolve over time independently. Thus, their joint state transition function is given by

$$f(\boldsymbol{x}_k, \boldsymbol{p}_k, \alpha_k, \epsilon_k | \boldsymbol{x}_{k-1}, \boldsymbol{p}_{k-1}, \alpha_{k-1}, \epsilon_{k-1}) \\ = f(\boldsymbol{p}_k|\boldsymbol{p}_{k-1}) f(\alpha_k|\alpha_{k-1}) f(\epsilon_k|\epsilon_{k-1}) \prod_{l\in\mathcal{L}_k} f\big(\underline{\boldsymbol{x}}_k^{(l)}|\boldsymbol{x}_{k-1}^{(l)}\big). \tag{7}$$

The state transition function of a PF $f(\underline{\boldsymbol{x}}_k^{(l)}|\boldsymbol{x}_{k-1}^{(l)}) = f(\underline{\boldsymbol{p}}_{\mathrm{VA},k}^{(l)}, \underline{r}_k^{(l)}|\boldsymbol{p}_{\mathrm{VA},k-1}^{(l)}, r_{k-1}^{(l)})$ will be elaborated in the following. If PF l does not exist at time $k-1$, i.e., $\mathsf{r}_{k-1}^{(l)} = 0$, it cannot exist at time k, i.e., $\underline{\mathsf{r}}_k^{(l)} = 0$, and thus its state PDF is $f_{\mathrm{D}}(\underline{\boldsymbol{p}}_{\mathrm{VA},k}^{(l)})$. This means that

$$f\big(\underline{\boldsymbol{p}}_{\mathrm{VA},k}^{(l)}, \underline{r}_k^{(l)}|\boldsymbol{p}_{\mathrm{VA},k-1}^{(l)}, 0\big) = \begin{cases} f_{\mathrm{D}}(\underline{\boldsymbol{p}}_{\mathrm{VA},k}^{(l)}), & \underline{r}_k^{(l)} = 0 \\ 0, & \underline{r}_k^{(l)} = 1. \end{cases} \tag{8}$$

However, if PF l existed at time $k-1$, i.e., $\mathsf{r}_{k-1}^{(l)} = 1$, then the probability that it still exists at time k, i.e., $\underline{\mathsf{r}}_k^{(l)} = 1$, is given by the survival probability $P_{\mathrm{s}}(\boldsymbol{p}_{\mathrm{VA},k}^{(l)})$, and if it still exists at time k, its state $\underline{\boldsymbol{p}}_{\mathrm{VA},k}^{(l)}$ remains unchanged. Thus,

$$f\big(\underline{\boldsymbol{p}}_{\mathrm{VA},k}^{(l)}, \underline{r}_k^{(l)}|\boldsymbol{p}_{\mathrm{VA},k-1}^{(l)}, 1\big) \\ = \begin{cases} \big(1 - P_{\mathrm{s}}(\boldsymbol{p}_{\mathrm{VA},k}^{(l)})\big) f_{\mathrm{D}}(\underline{\boldsymbol{p}}_{\mathrm{VA},k}^{(l)}), & \underline{r}_k^{(l)} = 0 \\ P_{\mathrm{s}}(\boldsymbol{p}_{\mathrm{VA},k}^{(l)}) \delta\big(\underline{\boldsymbol{p}}_{\mathrm{VA},k}^{(l)} - \boldsymbol{p}_{\mathrm{VA},k-1}^{(l)}\big), & \underline{r}_k^{(l)} = 1. \end{cases} \tag{9}$$

At $k = 1$, we assume that the set of legacy PFs is empty, i.e., $\mathcal{L}_1 = \emptyset$. For consistency, we formally define

$$f(\boldsymbol{x}_1, \boldsymbol{p}_1, \alpha_1, \epsilon_1 | \boldsymbol{x}_0, \boldsymbol{p}_0, \alpha_0, \epsilon_0) \triangleq f(\boldsymbol{p}_1) f(\alpha_1) f(\epsilon_1). \tag{10}$$

2) Association of Measurements With Features: Associating observed NLOS measurements to PFs is a necessary step for estimating the UE parameters and feature states. Data association can in principle be performed by making hard decisions on the feature-to-measurement associations. This can negatively affect the estimation accuracy if association decisions are erroneous. In this paper, we avoid hard decisions by considering probabilistic data association based on belief propagation (BP) [61], [62]. The corresponding association variables are introduced in what follows. We consider conventional data association, where a data association event is only valid if every feature can generate at most one measurement and every measurement originated from at most one feature.

Let $\mathsf{a}_k = [\mathsf{a}_k^{(1)}\ \mathsf{a}_k^{(2)} \cdots \mathsf{a}_k^{(L_K)}]^{\mathrm{T}}$ denote the feature-oriented data association vector at time k. The l^{th} entry $\mathsf{a}_k^{(l)}, l \in \mathcal{L}_k$ of a_k is the association variable of the l^{th} legacy PF $\underline{\mathsf{x}}_k^{(l)}$ and can take values $0, 1, \ldots, M_k$. In particular, $\mathsf{a}_k^{(l)} = j \in \mathcal{M}_k$ represents the case where the j^{th} measurement $\boldsymbol{z}_k^{(j)}$ originated from the l^{th} legacy PF. The case where the l^{th} PF did not generate a measurement (missed detection) is described by $\mathsf{a}_k^{(l)} = 0$. A feature-oriented data association vector a_k can only describe events where every PF generates at most one measurement. Following [53], we also introduce the measurement-oriented data association vector $\mathsf{b}_k = [\mathsf{b}_k^{(1)}\ \ \mathsf{b}_k^{(2)}\ \cdots\ \mathsf{b}_k^{(M_k)}]^{\mathrm{T}}$. The vector b_k contains one entry for each measurement where the j^{th} entry $\mathsf{b}_k^{(j)}$ takes values from $0, 1, \ldots, L_k$. Particularly, $\mathsf{b}_k^{(j)} = l \in \mathcal{L}_k$ means that the l^{th} legacy PF has generated the j^{th} measurement $\boldsymbol{z}_k^{(j)}$. If $\mathsf{b}_k^{(j)} = 0$, the measurement $\boldsymbol{z}_k^{(j)}$ did not originate from any legacy PF $\underline{\mathsf{x}}_k^{(l)}, l \in \mathcal{L}_k$, but it was generated by the new PF $\overline{\mathsf{x}}_k^{(j)}$ or by a false alarm. A measurement-oriented data association vector b_k can only describe events where every measurement was originated by at most one legacy PF. The relationship of a_k and b_k can be expressed by the following product of indicator functions

$$\Psi(\boldsymbol{a}_k, \boldsymbol{b}_k) = \prod_{l\in\mathcal{L}_k} \prod_{j\in\mathcal{M}_k} \psi_{l,j}\big(a_k^{(l)}, b_k^{(j)}\big) \tag{11}$$

where

$$\psi_{l,j}\big(a_k^{(l)}, b_k^{(j)}\big) \triangleq \begin{cases} 0, & a_k^{(l)} = j, b_k^{(j)} \neq l \\ & b_k^{(j)} = l, a_k^{(l)} \neq j \\ 1, & \text{otherwise.} \end{cases} \tag{12}$$

The factor $\Psi(\boldsymbol{a}_k, \boldsymbol{b}_k)$ is only equal to one if $\boldsymbol{a}_k$ and $\boldsymbol{b}_k$ describe the same valid data association event

3) Joint Posterior Distribution: For observed and thus fixed measurements $\mathbf{z}_{1:K}$, joint posterior distribution of the positions $\mathsf{p}_{1:K}$, orientations $\alpha_{1:K}$, clock offsets $\epsilon_{1:K}$ of the UE as well the feature states $\mathsf{x}_{1:K}$ and their associations $\mathsf{a}_{1:K}$ and $\mathsf{b}_{1:K}$ is given by (13) shown at the bottom of the next page and derived in Appendix A. It consists of the five terms described in what follows. The first term describes the evolution of the states of the UE and PFs from one time instance to the next one.

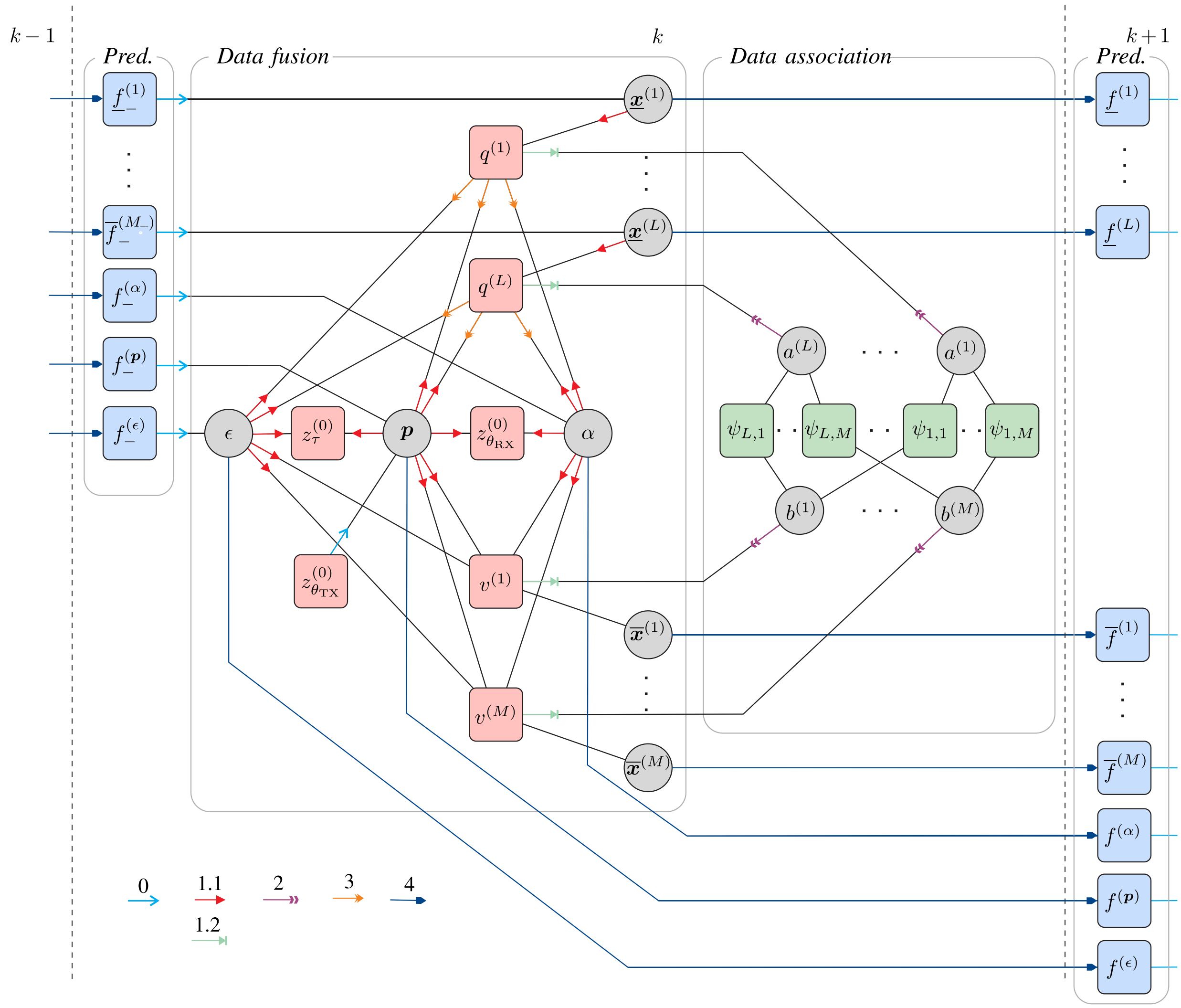

Fig. 6. Factor graph of the joint posterior distribution in (13) and message schedule. The factor graph can be sub-divided into the following three layers: *prediction*, *data fusion*, and *data association*. The prediction layer is responsible for the state transitions from the previous time step $k-1$ to the current time step k. All states (UE and PF states) are updated within the data fusion layer. Probabilistic data association, a preliminary step for completing data fusion, is performed iteratively in the data association layer. The message enumeration at the bottom left describes an important part of the schedule explained in Section IV-F. All messages are determined according the conventional BP rules [63], [64]. Pruning of PF states is not considered. The time indices k of factor and variable nodes have been omitted. The following shorthand notations have been used. *Prediction*: $L \triangleq L_k$, $L_{+} \triangleq L_{k+1}$, $\underline{f}_{-}^{(l)} \triangleq f(\underline{\boldsymbol{x}}_k^{(l)}|\boldsymbol{x}_{k-1}^{(l)})$, $f_{-}^{(\alpha)} \triangleq f(\alpha_k|\alpha_{k-1})$, $f_{-}^{(\epsilon)} \triangleq f(\epsilon_k|\epsilon_{k-1})$, $f_{-}^{(\boldsymbol{p})} \triangleq f(\boldsymbol{p}_k|\boldsymbol{p}_{k-1})$, $\underline{f}^{(l)} \triangleq f(\underline{\boldsymbol{x}}_{k+1}^{(l)}|\boldsymbol{x}_k^{(l)})$, $f^{(\alpha)} \triangleq f(\alpha_{k+1}|\alpha_k)$, $f^{(\epsilon)} \triangleq f(\epsilon_{k+1}|\epsilon_k)$, $f^{(\boldsymbol{p})} \triangleq f(\boldsymbol{p}_{k+1}|\boldsymbol{p}_k)$. *Data fusion*: $L \triangleq L_k$, $M \triangleq M_k$, $q^{(l)} \triangleq q(\underline{\boldsymbol{x}}_k^{(l)}, \boldsymbol{p}_k, \alpha_k, \epsilon_k, a_k^{(l)}; \boldsymbol{z}_k)$, $v^{(j)} \triangleq v(\overline{\boldsymbol{x}}_k^{(j)}, \boldsymbol{p}_k, \alpha_k, \epsilon_k, b_k^{(j)}; \boldsymbol{z}_k^{(j)})$, $z_{\tau}^{(0)} \triangleq f(z_{\tau,k}^{(0)}|\boldsymbol{p}_k, \epsilon_k)$, $z_{\theta_{\mathrm{RX}}}^{(0)} \triangleq f(z_{\theta_{\mathrm{RX}},k}^{(0)}|\boldsymbol{p}_k, \alpha_k)$, $z_{\theta_{\mathrm{TX}}}^{(0)} \triangleq f(z_{\theta_{\mathrm{TX}},k}^{(0)}|\boldsymbol{p}_k)$. *Data association*: $\psi_{l,j} \triangleq \psi_{l,j}(a_k^{(l)}, b_k^{(j)})$.

$$
\begin{aligned}
f(\boldsymbol{p}_{1:K}, \boldsymbol{\alpha}_{1:K}, \boldsymbol{\epsilon}_{1:K}, \boldsymbol{x}_{1:K}, \boldsymbol{a}_{1:K}, \boldsymbol{b}_{1:K}|\boldsymbol{z}_{1:K}) = \prod_{k=1}^{K} & \underbrace{f(\boldsymbol{p}_k|\boldsymbol{p}_{k-1}) f(\alpha_k|\alpha_{k-1}) f(\epsilon_k|\epsilon_{k-1}) \prod_{l\in\mathcal{L}_k} f(\underline{\boldsymbol{x}}_k^{(l)}|\boldsymbol{x}_{k-1}^{(l)})}_{\text{state transition term}} \\
& \times \underbrace{\prod_{l\in\mathcal{L}_k} q(\underline{\boldsymbol{x}}_k^{(l)}, \boldsymbol{p}_k, \alpha_k, \epsilon_k, a_k^{(l)}; \boldsymbol{z}_k)}_{\text{old features-UE-NLOS term}} \underbrace{\prod_{j\in\mathcal{M}_k} v(\overline{\boldsymbol{x}}_k^{(j)}, \boldsymbol{p}_k, \alpha_k, \epsilon_k, b_k^{(j)}; \boldsymbol{z}_k)}_{\text{new features-UE-NLOS term}} \\
& \times \underbrace{\prod_{l\in\mathcal{L}_k} \prod_{j\in\mathcal{M}_k} \psi_{l,j}(a_k^{(l)}, b_k^{(j)})}_{\text{feature association term}} \underbrace{f(z_{\tau,k}^{(0)}|\boldsymbol{p}_k, \epsilon_k) f(z_{\theta_{\mathrm{RX}},k}^{(0)}|\boldsymbol{p}_k, \alpha_k) f(z_{\theta_{\mathrm{TX}},k}^{(0)}|\boldsymbol{p}_k)}_{\text{UE-LOS term}}
\end{aligned}
\tag{13}
$$

Interactions between the NLOS measurements, the UE states, and the legacy and new PFs are characterized by the second and third term, respectively. Here, the factors $q(\underline{\boldsymbol{x}}_k^{(l)}, \boldsymbol{p}_k, \alpha_k, \epsilon_k, a_k^{(l)}; \boldsymbol{z}_k) = q(\underline{\boldsymbol{p}}_{\mathrm{VA},k}^{(l)}, \underline{r}_k^{(l)}, \boldsymbol{p}_k, \alpha_k, \epsilon_k, a_k^{(l)}; \boldsymbol{z}_k)$ are defined as

$$q\big(\underline{\boldsymbol{p}}_{\mathrm{VA},k}^{(l)}, 1, \boldsymbol{p}_k, \alpha_k, \epsilon_k, a_k^{(l)}; \boldsymbol{z}_k\big) \triangleq \begin{cases} \dfrac{P_{\mathrm{d}}(\underline{\boldsymbol{p}}_{\mathrm{VA},k}^{(l)}, \boldsymbol{p}_k, \alpha_k) f(\boldsymbol{z}_k^{(j)} | \underline{\boldsymbol{p}}_{\mathrm{VA},k}^{(l)}, \boldsymbol{p}_k, \epsilon_k, \alpha_k)}{m_{\mathrm{c}} f_{\mathrm{c}}(\boldsymbol{z}_k^{(j)})}, & a_k^{(l)} \neq 0 \\ 1 - P_{\mathrm{d}}(\underline{\boldsymbol{p}}_{\mathrm{VA},k}^{(l)}, \boldsymbol{p}_k, \alpha_k), & a_k^{(l)} = 0 \end{cases} \tag{14}$$

(where $a_k^{(l)} \neq 0$ is equal to $a_k^{(l)} = j \in \mathcal{M}_k$) and

$$q\big(\underline{\boldsymbol{p}}_{\mathrm{VA},k}^{(l)}, 0, \boldsymbol{p}_k, \alpha_k, \epsilon_k, a_k^{(l)}; \boldsymbol{z}_k\big) \triangleq \mathbb{I}\big(a_k^{(l)}\big). \tag{15}$$

Similarly, $v(\overline{\boldsymbol{x}}_k^{(j)}, \boldsymbol{p}_k, \alpha_k, \epsilon_k, b_k^{(j)}; \boldsymbol{z}_k^{(j)}) = v(\overline{\boldsymbol{p}}_{\mathrm{VA},k}^{(j)}, \overline{r}_k^{(j)}, \boldsymbol{p}_k, \alpha_k, \epsilon_k, b_k^{(j)}; \boldsymbol{z}_k^{(j)})$ is given by

$$v\big(\overline{\boldsymbol{p}}_{\mathrm{VA},k}^{(j)}, 1, \boldsymbol{p}_k, \alpha_k, \epsilon_k, b_k^{(j)}; \boldsymbol{z}_k^{(j)}\big) \triangleq \frac{\lambda_{\mathrm{n},k}(\overline{\boldsymbol{p}}_{\mathrm{VA},k}^{(j)}) f(\boldsymbol{z}_k^{(j)} | \overline{\boldsymbol{p}}_{\mathrm{VA},k}^{(j)}, \boldsymbol{p}_k, \epsilon_k, \alpha_k) \mathbb{I}(b_k^{(j)})}{m_{\mathrm{c}} f_{\mathrm{c}}(\boldsymbol{z}_k^{(j)})} \tag{16}$$

and

$$v\big(\overline{\boldsymbol{p}}_{\mathrm{VA},k}^{(j)}, 0, \boldsymbol{p}_k, \alpha_k, \epsilon_k, b_k^{(j)}; \boldsymbol{z}_k^{(j)}\big) \triangleq f_{\mathrm{D}}\big(\overline{\boldsymbol{p}}_{\mathrm{VA},k}^{(j)}\big). \tag{17}$$

The forth term describes the associations of measurements with PFs. Mathematically, it is given by (11) and (12). Finally, the fifth term encodes the relationship of the UE states and the measurements $\boldsymbol{z}_k^{(0)} \triangleq [z_{\theta_{\mathrm{RX}},k}^{(0)} \quad z_{\theta_{\mathrm{TX}},k}^{(0)} \quad z_{\tau,k}^{(0)}]^{\mathrm{T}}$ of the LOS path. Note that the existence of the LOS link increases the UE state estimation accuracy but it is not required for localization, synchronization, and mapping. In case that the LOS is obstructed at any time instance k, the corresponding terms in (13) equal one, i.e., $f(z_{\theta_{\mathrm{RX}},k}^{(0)} | \boldsymbol{p}_k, \alpha_k) f(z_{\theta_{\mathrm{TX}},k}^{(0)} | \boldsymbol{p}_k) f(z_{\tau,k}^{(0)} | \boldsymbol{p}_k, \epsilon_k) = 1$. Note that a LOS measurement at time $k = 1$ is not necessary, but it can significantly improve the convergence speed of COMPAS.

C. *Factor Graph of the Joint Posterior Distribution*

The factor graph representing the factorization in (13) is depicted in Fig. 6. Note that – as it is common for factor graphs – this factorization is not unique. One could change the structure of the graph by merging or splitting factor and variable nodes. However, the considered factorization reveals an interesting structure that consists of *prediction*, *data fusion*, and *data association* layers. COMPAS will use this structure for inference, as will be discussed next.

IV. COMPAS: An Inference Engine for Situational-Awareness

In this section we present COMPAS; a message passing-based inference engine that is based on the stochastic model and factor graph developed in the previous section. COMPAS was derived using conventional BP rules [63], [64], sending BP messages only forward in time [53], and by employing the message schedule presented in Section IV-F at each time step.

A. *Joint Detection and Estimation*

Our goal is to estimate the UE states (p_k, α_k, and ϵ_k) and to infer the PF states $\mathsf{x}_k^{(l)}$. Inferring the PF states includes detecting their state of existence and estimating their positions subsequently. Hereafter, PF detection will be termed *target declaration* to avoid confusion with the detection performed by the channel estimator. Declaring the existence of PFs and estimating their positions as well as estimating the states of the UE are based on the marginal posterior PDFs of the UE and PF states. For example, at time k the marginal posterior of p_k is given by $f(\boldsymbol{p}_k | \boldsymbol{z}_{1:k})$. We approximate these marginal posteriors by means of BP. The approximated marginals are termed beliefs and denoted by $b(\boldsymbol{p}_k) \approx f(\boldsymbol{p}_k | \boldsymbol{z}_{1:k})$. For estimation, the minimum mean square error (MMSE) criterion is employed. For instance, the UE position estimate is given by $\hat{\boldsymbol{p}}_k^{\mathrm{MMSE}} \approx \int \boldsymbol{p}_k b(\boldsymbol{p}_k) \mathrm{d}\boldsymbol{p}_k$. In order to infer the state of a PF, we first have to detect its state of existence based on its posterior existence probability $\mathbb{P}(\mathsf{r}_k^{(l)} = 1) \approx \int b(\boldsymbol{p}_{\mathrm{VA},k}^{(l)}, 1) \mathrm{d}\boldsymbol{p}_{\mathrm{VA},k}^{(l)}$, where $b(\boldsymbol{p}_{\mathrm{VA},k}^{(l)}, r_k^{(l)})$ is the belief of the l^{th} PF. In particular, we declare the existence of a PF l if its posterior existence probability exceeds the threshold P_{ex}, i.e., $\mathbb{P}(\mathsf{r}_k^{(l)} = 1) > P_{\mathrm{ex}}$. The position of a PF l is finally estimated as $\hat{\boldsymbol{p}}_{\mathrm{VA},k}^{(l)\mathrm{MMSE}} \approx \int \boldsymbol{p}_{\mathrm{VA},k}^{(l)} b(\boldsymbol{p}_{\mathrm{VA},k}^{(l)} | 1) \mathrm{d}\boldsymbol{p}_{\mathrm{VA},k}^{(l)}$, where $b(\boldsymbol{p}_{\mathrm{VA},k}^{(l)} | 1) = b(\boldsymbol{p}_{\mathrm{VA},k}^{(l)}, 1) / \mathbb{P}(\mathsf{r}_k^{(l)} = 1)$.

B. *Initialization*

At time $k = 1$, we assume (see Section II-A) that only the intensity function of newly detected features $\lambda_{\mathrm{n},1}(\check{\boldsymbol{p}}_{\mathrm{VA},1})$ is available as prior information regarding the features in the propagation environment. Moreover, the set of legacy PFs is empty, i.e., $\mathcal{L}_1 = \emptyset$. In addition, potentially uninformative prior information regarding the position, orientation and clock offset of the UE is available. The angle-based channel estimator generates M_1 measurements as outlined in Fig. 3, where each measurement $\boldsymbol{z}_1^{(j)}, j \in \mathcal{M}_1 = \{1, 2, \ldots, M_1\}$ could be generated by an actual feature or clutter. Thus, M_1 new PFs are added to the state space as shown in Fig. 4.

In order to infer the states (position and existence) of every new PF $\overline{\mathsf{x}}_1^{(j)}$, the message[5] $\mu_{f_{v(j)} \to \overline{\boldsymbol{x}}_1^{(j)}}$ must be determined for each PF. This message is computed based on incoming messages to $v^{(j)}$. From the factor graph in Fig. 6, it can be observed that the factor node $v^{(j)}$ has one incoming message per UE state (red arrows) and one incoming message from the DA layer (magenta arrow). Note that data association is not necessary at $k = 1$ since the set of legacy PFs is empty, i.e., $|\mathcal{L}_1| = 0$. Hence only the incoming messages from the UE states are considered. Consequently, the incoming messages to the factor node $v^{(j)}$ are the priors on the UE states, i.e., $\mu_{\boldsymbol{p}_1 \to f_{v(j)}}(\boldsymbol{p}_1) = f(\boldsymbol{p}_1)$, $\mu_{\alpha_1 \to f_{v(j)}}(\alpha_1) = f(\alpha_1)$, and $\mu_{\epsilon_1 \to f_{v(j)}}(\epsilon_1) = f(\epsilon_1), \forall j \in \mathcal{M}_1 = \{1, 2, \ldots, M_1\}$.

Recall that the state variable of a new PF j involves a continuous state (the 2D position $\overline{\mathsf{p}}_{\mathrm{VA},1}^{(j)}$) and a discrete state (the binary

[5]For notational simplicity, the iteration indices of BP-messages are omitted.

existence variable $\bar{\mathsf{r}}_1^{(j)} \in \{0,1\}$). For each of the two values of $\bar{\mathsf{r}}_1^{(j)}$, the outgoing message $\mu_{v^{(j)} \to \overline{\boldsymbol{x}}_1^{(j)}}(\overline{\boldsymbol{p}}_{\mathrm{VA},1}^{(j)}, \bar{r}_1^{(j)})$ from the factor node $v^{(j)}$ is a different continuous function of $\overline{\boldsymbol{p}}_{\mathrm{VA},1}^{(j)}$, i.e.,

$$\begin{aligned}
&\mu_{v^{(j)} \to \overline{\boldsymbol{x}}_1^{(j)}}(\overline{\boldsymbol{p}}_{\mathrm{VA},1}^{(j)}, 1) \\
&\quad = \iiint v\big(\overline{\boldsymbol{p}}_{\mathrm{VA},1}^{(j)}, 1, \boldsymbol{p}_1, \alpha_1, \epsilon_1, 0; \boldsymbol{z}_1^{(j)}\big) \\
&\qquad \times f(\alpha_1) f(\epsilon_1) f(\boldsymbol{p}_1) \mathrm{d}\boldsymbol{p}_1 \mathrm{d}\alpha_1 \mathrm{d}\epsilon_1
\end{aligned} \tag{18}$$

and

$$\begin{aligned}
&\mu_{v^{(j)} \to \overline{\boldsymbol{x}}_1^{(j)}}(\overline{\boldsymbol{p}}_{\mathrm{VA},1}^{(j)}, 0) \\
&\quad = \iiint v\big(\overline{\boldsymbol{p}}_{\mathrm{VA},1}^{(j)}, 0, \boldsymbol{p}_1, \alpha_1, \epsilon_1, 0; \boldsymbol{z}_1^{(j)}\big) \\
&\qquad \times f(\alpha_1) f(\epsilon_1) f(\boldsymbol{p}_1) \mathrm{d}\boldsymbol{p}_1 \mathrm{d}\alpha_1 \mathrm{d}\epsilon_1 \\
&\quad = f_{\mathrm{D}}\big(\overline{\boldsymbol{p}}_{\mathrm{VA},1}^{(j)}\big)
\end{aligned} \tag{19}$$

where we used (17) to obtain the last line in (19). The message $\mu_{v^{(j)} \to \overline{\boldsymbol{x}}_1^{(j)}}(\overline{\boldsymbol{p}}_{\mathrm{VA},1}^{(j)}, \bar{r}_1^{(j)})$ also constitutes the belief $b(\overline{\boldsymbol{x}}_1^{(j)})$ that is forwarded to the next time step $k = 2$. UE states are not updated based on new PFs. Since the UE states are not observable only based on the LOS measurements [51], the beliefs are given by the priors, e.g., $b(\boldsymbol{p}_1) = f(\boldsymbol{p}_1)$.

C. State Transition

Transferring states from time step $k-1$ to time step k requires predicting the states based on their state transition models. UE prediction messages are obtained by message filtering, e.g.,

$$\mu_{f_-^{(\boldsymbol{p})} \to \boldsymbol{p}_k}(\boldsymbol{p}_k) = \int f(\boldsymbol{p}_k | \boldsymbol{p}_{k-1}) \mu_{\boldsymbol{p}_{k-1} \to f_-^{(\boldsymbol{p})}}(\boldsymbol{p}_{k-1}) \mathrm{d}\boldsymbol{p}_{k-1}. \tag{20}$$

For the UE parameters $\mathsf{\alpha}_k$ and $\mathsf{\epsilon}_k$, messages are obtained similarly. Note that since we send BP messages only forward in time, the incoming message to the prediction node is at the same time the belief, e.g, $\mu_{\boldsymbol{p}_{k-1} \to f_-^{(\boldsymbol{p})}}(\boldsymbol{p}_{k-1}) = b(\boldsymbol{p}_{k-1})$. This implies that the incoming and outgoing messages (e.g., $\mu_{\boldsymbol{p}_{k-1} \to f_-^{(\boldsymbol{p})}}(\boldsymbol{p}_{k-1})$ and $\mu_{f_-^{(\boldsymbol{p})} \to \boldsymbol{p}_k}(\boldsymbol{p}_k)$) integrate to one.

The prediction messages for legacy PFs, $l \in \mathcal{L}_k$ are given by

$$\begin{aligned}
\mu_{f_-^{(l)} \to \underline{\boldsymbol{x}}_k^{(l)}}(\underline{\boldsymbol{x}}_k^{(l)}) &= \int \sum_{r_{k-1}^{(l)} \in \{0,1\}} f\big(\underline{\boldsymbol{p}}_{\mathrm{VA},k}^{(l)}, \underline{r}_k^{(l)} | \boldsymbol{p}_{\mathrm{VA},k-1}^{(l)}, r_{k-1}^{(l)}\big) \\
&\quad \times \mu_{\boldsymbol{x}_{k-1}^{(l)} \to f_-^{(l)}}\big(\boldsymbol{p}_{\mathrm{VA},k-1}^{(l)}, r_{k-1}^{(l)}\big) \mathrm{d}\boldsymbol{p}_{\mathrm{VA},k-1}^{(l)}
\end{aligned}$$

with $f(\underline{\boldsymbol{p}}_{\mathrm{VA},k}^{(l)}, \underline{r}_k^{(l)} | \boldsymbol{p}_{\mathrm{VA},k-1}^{(l)}, r_{k-1}^{(l)})$ as provided in (8) and (9). Again, the two cases of $\underline{\mathsf{r}}_k^{(l)} \in \{0,1\}$ have to be considered. For $\underline{\mathsf{r}}_k^{(l)} = 1$, we obtain

$$\begin{aligned}
&\mu_{f_-^{(l)} \to \underline{\boldsymbol{x}}_k^{(l)}}\big(\underline{\boldsymbol{p}}_{\mathrm{VA},k}^{(l)}, 1\big) \\
&\quad = P_{\mathrm{s}}\big(\boldsymbol{p}_{\mathrm{VA},k}^{(l)}\big) \mu_{\boldsymbol{x}_{k-1}^{(l)} \to f_-^{(l)}}\big(\boldsymbol{p}_{\mathrm{VA},k-1}^{(l)} = \underline{\boldsymbol{p}}_{\mathrm{VA},k}^{(l)}, 1\big)
\end{aligned} \tag{21}$$

where we used the shifting property of the Dirac delta function (cf. (9)) to perform the integration. Similarly, for $\underline{\mathsf{r}}_k^{(l)} = 0$, we get $\mu_{f_-^{(l)} \to \underline{\boldsymbol{x}}_k^{(l)}}(\underline{\boldsymbol{p}}_{\mathrm{VA},k}^{(l)}, 0) = f_{\mathrm{D}}(\underline{\boldsymbol{p}}_{\mathrm{VA},k}^{(l)}) P_{\mathrm{pred},k}^{(l)}$ where $P_{\mathrm{pred},k}^{(l)}$ is the predicted probability of non-existence of a PF l at time k that is given by

$$\begin{aligned}
P_{\mathrm{pred},k}^{(l)} &= \int \big(1 - P_{\mathrm{s}}(\boldsymbol{p}_{\mathrm{VA},k}^{(l)})\big) \mu_{\boldsymbol{x}_{k-1}^{(l)} \to f_-^{(l)}}\big(\boldsymbol{p}_{\mathrm{VA},k-1}^{(l)}, 1\big) \\
&\quad + \mu_{\boldsymbol{x}_{k-1}^{(l)} \to f_-^{(l)}}\big(\boldsymbol{p}_{\mathrm{VA},k-1}^{(l)}, 0\big) \mathrm{d}\boldsymbol{p}_{\mathrm{VA},k-1}^{(l)}.
\end{aligned} \tag{22}$$

Remark: In order to propagate PFs forward in time, only their probability of existence must be updated. The reason is that the reflecting surfaces and the BS are assumed to be static and thus, the positions of these VAs do not change. Updating their existence probabilities requires evaluating four possibilities: (i) $\mathsf{r}_{k-1}^{(l)} = 1 \to \underline{\mathsf{r}}_k^{(l)} = 1$, (ii) $\mathsf{r}_{k-1}^{(l)} = 0 \to \underline{\mathsf{r}}_k^{(l)} = 1$, (iii) $\mathsf{r}_{k-1}^{(l)} = 1 \to \underline{\mathsf{r}}_k^{(l)} = 0$, and (iv) $\mathsf{r}_{k-1}^{(l)} = 0 \to \underline{\mathsf{r}}_k^{(l)} = 0$. The first two cases are described in (21), where the term $P_{\mathrm{s}}(\boldsymbol{p}_{\mathrm{VA},k}^{(l)}) \mu_{\boldsymbol{x}_{k-1} \to f_-^{(l)}}(\underline{\boldsymbol{p}}_{\mathrm{VA},k}^{(l)} = \boldsymbol{p}_{\mathrm{VA},k-1}^{(l)}, 1)$ reflects case (i) and the second case (ii) has probability zero. The first term in (21) reduces the probability of existence by the survival probability $P_{\mathrm{s}}(\boldsymbol{p}_{\mathrm{VA},k}^{(l)}) < 1$. In other words, the PDF of the location of the PF remains unchanged and the probability of existence of the PF is decreased by the factor $P_{\mathrm{s}}(\boldsymbol{p}_{\mathrm{VA},k}^{(l)})$. Case (ii), where an existing legacy PF did not exist at $k-1$ but does exist at k, cannot occur. Hence the probability is zero.[6] The cases (iii) and (iv) are described by the first and second term in (22), respectively. The first term is weighted with the probability $(1 - P_{\mathrm{s}}(\boldsymbol{p}_{\mathrm{VA},k}^{(l)}))$ that the PF did not survive the state-transition and the second term reflects the probability that the PF neither existed at $k-1$ nor exists at k.

D. Data Association

Before updating the states of the UE and the PFs, the NLOS measurements must be associated with the legacy and new PFs. The DA layer computes the probabilistic associations based on the incoming messages $\mu_{q^{(l)} \to a_k^{(l)}}(a_k^{(l)})$, $a_k^{(l)} \in \{0, 1, \ldots, M_k\}$, $l \in \mathcal{L}_k$ from legacy PFs and the messages $\mu_{v^{(j)} \to b_k^{(j)}}(b_k^{(j)})$, $b_k^{(j)} \in \{0, 1, \ldots, L_k\}$, $j \in \mathcal{M}_k$ from new PFs. These messages are determined by integrating and summing over all variables except $a_k^{(l)}$ and $b_k^{(j)}$, respectively. In particular, the message from the l^{th} legacy PF $\underline{\boldsymbol{x}}_k^{(l)}$ is given by

$$\begin{aligned}
&\mu_{q^{(l)} \to a_k^{(l)}}\big(a_k^{(l)}\big) \\
&\quad = \sum_{\underline{r}_k^{(l)} \in \{0,1\}} \iiiint q\big(\underline{\boldsymbol{p}}_{\mathrm{VA},k}^{(l)}, \underline{r}_k^{(l)}, \boldsymbol{p}_k, \alpha_k, \epsilon_k, a_k^{(l)}; \boldsymbol{z}_k\big) \\
&\qquad \times \mu_{\underline{\boldsymbol{x}}_k^{(l)} \to q^{(l)}}(\underline{\boldsymbol{x}}_k^{(l)}) \mu_{\boldsymbol{p}_k \to q^{(l)}}\big(\boldsymbol{p}_k\big) \mu_{\alpha_k \to q^{(l)}}(\alpha_k) \\
&\qquad \times \mu_{\epsilon_k \to q^{(l)}}(\epsilon_k) \mathrm{d}\underline{\boldsymbol{p}}_{\mathrm{VA},k}^{(l)} \mathrm{d}\boldsymbol{p}_k \mathrm{d}\alpha_k \mathrm{d}\epsilon_k.
\end{aligned} \tag{23}$$

[6] As discussed in Section III-A, actual features that are detected for the first time are modeled by a new PF.

Performing the summation over $\underline{r}_k^{(l)} \in \{0,1\}$ and using $q(\underline{\boldsymbol{p}}_{\mathrm{VA},k}^{(l)}, 0, \boldsymbol{p}_k, \alpha_k, \epsilon_k, a_k^{(l)}; \boldsymbol{z}_k)$ as in (15) yields

$$\begin{aligned}\mu_{q^{(l)}\to a_k^{(l)}}\big(a_k^{(l)}\big) &= \iiiint q\big(\underline{\boldsymbol{p}}_{\mathrm{VA},k}^{(l)}, 1, \boldsymbol{p}_k, \alpha_k, \epsilon_k, a_k^{(l)}; \boldsymbol{z}_k\big) \\ &\quad \times \mu_{\underline{\boldsymbol{x}}_k^{(l)}\to q^{(l)}}\big(\underline{\boldsymbol{p}}_{\mathrm{VA},k}^{(l)}, 1\big)\mu_{\boldsymbol{p}_k\to q^{(l)}}(\boldsymbol{p}_k)\mu_{\alpha_k\to q^{(l)}}(\alpha_k) \\ &\quad \times \mu_{\epsilon_k\to q^{(l)}}(\epsilon_k)\mathrm{d}\underline{\boldsymbol{p}}_{\mathrm{VA},k}^{(l)}\mathrm{d}\boldsymbol{p}_k\mathrm{d}\alpha_k\mathrm{d}\epsilon_k + \mathbb{I}\big(a_k^{(l)}\big)P_{\mathrm{pred},k}^{(l)}. \end{aligned} \tag{24}$$

The message from the j^{th} new PF is given by a similar expression as in (23) that involves a summation over $\overline{r}_k^{(l)} \in \{0,1\}$. By performing the same steps as in the calculation of (24) and using the expression for $v(\overline{\boldsymbol{p}}_{\mathrm{VA}}^{(l)}, 0, \boldsymbol{p}_k, \alpha_k, \epsilon_k, b_k^{(j)}; \boldsymbol{z}_k)$ in (17), we directly obtain

$$\begin{aligned}\mu_{v^{(j)}\to b_k^{(j)}}\big(b_k^{(j)}\big) &= \mathbb{I}\big(b_k^{(j)}\big) \iiiint v\big(\overline{\boldsymbol{p}}_{\mathrm{VA},k}^{(l)}, 1, \boldsymbol{p}_k, \alpha_k, \epsilon_k, b_k^{(j)}; \boldsymbol{z}_k\big) \\ &\quad \times \mu_{\overline{\boldsymbol{x}}_k^{(l)}\to v^{(j)}}\big(\overline{\boldsymbol{p}}_{\mathrm{VA},k}^{(l)}, 1\big)\mu_{\boldsymbol{p}_k\to v^{(j)}}(\boldsymbol{p}_k)\mu_{\alpha_k\to v^{(j)}}(\alpha_k) \\ &\quad \times \mu_{\epsilon_k\to v^{(j)}}(\epsilon_k)\mathrm{d}\overline{\boldsymbol{p}}_{\mathrm{VA},k}^{(l)}\mathrm{d}\boldsymbol{p}_k\mathrm{d}\alpha_k\mathrm{d}\epsilon_k + 1. \end{aligned} \tag{25}$$

The messages (24) and (25) are the input to the DA layer as shown in Fig. 6. Probabilistic data association is performed iteratively by passing messages between the nodes $a_k^{(l)}, l \in \mathcal{L}_k$ and $b_k^{(j)}, j \in \mathcal{M}_k$. After N_{DA} iterations inside the DA layer, the outgoing messages $\mu_{a_k^{(l)}\to q^{(l)}}(a_k^{(l)})$ and $\mu_{b_k^{(j)}\to v^{(j)}}(b_k^{(j)})$ are passed back to the data fusion layer. The message passing routine in the data association layer is provided in [53, Section VI].

E. Data Fusion

Based on the probabilistic associations from the DA layer, the states of the UE and the PFs are updated based on the LOS $\boldsymbol{z}_k^{(0)}$ and NLOS $\boldsymbol{z}_k^{(j)}, j \in \mathcal{M}_k$ measurements. However, no messages are being sent back from the factor nodes $v^{(j)}, j \in \mathcal{M}_k$ of new PFs. In the first iteration inside the data fusion layer, the predicted states from the previous time step are, at the same time, the outgoing messages from the variable nodes, e.g., $\mu_{\epsilon_k\to z_{\tau,k}^{(0)}}(\epsilon_k) = \mu_{f_-^{(\epsilon)}\to\epsilon_k}(\epsilon_k)$. In subsequent iterations, outgoing messages from variable nodes are determined as the product of all incoming messages except for that of the factor node for which the message is computed [63], [64], e.g., $\mu_{\epsilon_k\to z_{\tau,k}^{(0)}}(\epsilon_k) = \mu_{f_-^{(\epsilon)}\to\epsilon_k}(\epsilon_k)\prod_{l\in\mathcal{L}_k}\mu_{q^{(l)}\to\epsilon_k}(\epsilon_k)$. The outgoing message from the LOS factor node $z_{\tau,k}^{(0)}$ is given by

$$\mu_{z_{\tau,k}^{(0)}\to\boldsymbol{p}_k}(\boldsymbol{p}_k) = \int f\big(z_{\tau,k}^{(0)}|\boldsymbol{p}_k, \epsilon_k\big)\mu_{\epsilon_k\to z_{\tau,k}^{(0)}}(\epsilon_k)\mathrm{d}\epsilon_k. \tag{26}$$

Similar expressions are obtained for outgoing messages of the LOS factor nodes $z_{\theta_{\mathrm{RX}},k}^{(0)}$ and $z_{\theta_{\mathrm{TX}},k}^{(0)}$.

Due to the data association uncertainty of NLOS measurements, PFs are associated with measurements in a probabilistic manner. This probabilistic association results in an additional summation over all possible association events $\mathsf{a}_k^{(l)} \in \{0, 1, \ldots, M_k\}$. For instance, the message $\mu_{q^{(l)}\to\boldsymbol{p}_k}(\boldsymbol{p}_k)$ from $q^{(l)}$ to $\boldsymbol{p}_k$ is given by

$$\begin{aligned}\mu_{q^{(l)}\to\boldsymbol{p}_k}(\boldsymbol{p}_k) &= \sum_{\underline{\mathsf{r}}_k^{(l)}\in\{0,1\}}\sum_{\mathsf{a}_k^{(l)}=0}^{M_k}\iiint q\big(\underline{\boldsymbol{p}}_{\mathrm{VA},k}^{(l)}, \underline{r}_k^{(l)}, \boldsymbol{p}_k, \alpha_k, \epsilon_k, a_k^{(l)}; \boldsymbol{z}_k\big) \\ &\quad \times \mu_{\underline{\boldsymbol{x}}_k^{(l)}\to q^{(l)}}\big(\underline{\boldsymbol{p}}_{\mathrm{VA},k}^{(l)}, \underline{r}_k^{(l)}\big)\mu_{\alpha_k\to q^{(l)}}(\alpha_k)\mu_{\epsilon_k\to q^{(l)}}(\epsilon_k) \\ &\quad \times \mu_{a_k^{(l)}\to q^{(l)}}\big(a_k^{(l)}\big)\mathrm{d}\underline{\boldsymbol{p}}_{\mathrm{VA},k}^{(l)}\mathrm{d}\alpha_k\mathrm{d}\epsilon_k \end{aligned} \tag{27}$$

where $\mu_{a_k^{(l)}\to q^{(l)}}(a_k^{(l)})$ is an outgoing message from the DA layer. All other messages that leave the factor node $q^{(l)}$ towards UE states have a similar structure compared to that presented in (27). Beliefs are computed as the product of all incoming messages, e.g., $b(\boldsymbol{p}_k) = \mu_{f_-^{(\boldsymbol{p})}\to\boldsymbol{p}_k}(\boldsymbol{p}_k)\mu_{z_{\tau,k}^{(0)}\to\boldsymbol{p}_k}(\boldsymbol{p}_k)\mu_{z_{\theta_{\mathrm{RX}},k}^{(0)}\to\boldsymbol{p}_k}(\boldsymbol{p}_k)\mu_{z_{\theta_{\mathrm{TX}},k}^{(0)}\to\boldsymbol{p}_k}(\boldsymbol{p}_k) \times \prod_{l\in\mathcal{L}_k}\mu_{q^{(l)}\to\boldsymbol{p}_k}(\boldsymbol{p}_k)$.

The states of PFs are updated based on the messages from the factor nodes $q^{(l)}, l \in \mathcal{L}_k$ and $v^{(j)}, j \in \mathcal{M}_k$. The messages $\mu_{v^{(j)}\to\overline{\boldsymbol{x}}_k^{(j)}}(\overline{\boldsymbol{x}}_k^{(j)}), j \in \mathcal{M}_k$ of new PFs can be obtained by replacing the priors $f(\alpha_1)$, $f(\epsilon_1)$, and $f(\boldsymbol{p}_1)$ in (18) and (19) by the incoming messages to $v^{(j)}$, i.e., by $\mu_{\alpha_k\to v^{(j)}}(\alpha_k)$, $\mu_{\epsilon_k\to v^{(j)}}(\epsilon_k)$, and $\mu_{\boldsymbol{p}_k\to v^{(j)}}(\boldsymbol{p}_k)$, respectively. Similar expressions can be obtained for the messages $\mu_{q^{(l)}\to\underline{\boldsymbol{x}}_k^{(l)}}(\underline{\boldsymbol{x}}_k^{(l)}), l \in \mathcal{L}_k$ related to legacy PFs. The beliefs of new PFs are directly given by the messages $\mu_{v^{(j)}\to\overline{\boldsymbol{x}}_k^{(j)}}(\overline{\boldsymbol{x}}_k^{(j)}), j \in \mathcal{M}_k$, i.e., $b(\overline{\boldsymbol{x}}_k^{(j)}) \propto \mu_{v^{(j)}\to\overline{\boldsymbol{x}}_k^{(j)}}(\overline{\boldsymbol{x}}_k^{(j)})$. For legacy PFs, the beliefs are given as the product of $\mu_{q^{(l)}\to\underline{\boldsymbol{x}}_k^{(l)}}(\underline{\boldsymbol{x}}_k^{(l)})$ and the messages from the prediction layer, i.e., $b(\underline{\boldsymbol{x}}_k^{(l)}) \propto \mu_{f_-^{(l)}\to\underline{\boldsymbol{x}}_k^{(l)}}(\underline{\boldsymbol{x}}_k^{(l)})\mu_{q^{(l)}\to\underline{\boldsymbol{x}}_k^{(l)}}(\underline{\boldsymbol{x}}_k^{(l)}), l \in \mathcal{L}_k$. Note that all beliefs must be valid PDFs in the sense that their probability mass equals one. This may require an additional normalization step which is not explicitly shown.

Let us discuss the messages that leave the factor nodes $q^{(l)}$ towards the state variables of the UE and legacy PFs. For instance, the message $\mu_{q^{(l)}\to\boldsymbol{p}_k}(\boldsymbol{p}_k)$ in (27) contains two sums. The first sum accounts for the fact that the l^{th} legacy PF could or could not exist. The second sum accounts for the fact the l^{th} legacy PF could have generated no measurement ($\mathsf{a}_k^{(l)} = 0$) or any one of the observed measurements $\boldsymbol{z}_k^{(j)}, j \in \{1, 2, \ldots, M_k\}$. The message $\mu_{a_k^{(l)}\to q^{(l)}}(a_k^{(l)}), \mathsf{a}_k^{(l)} \in \{0, 1, \ldots, M_k\}$ weights each of these association hypotheses.

F. Schedule and Practical Considerations

The sequence of passed messages at any time step $k > 1$ is indicated in Fig. 6. Message passing starts with the outgoing messages in the *prediction layer* and the message from the AOD node $z_{\theta_{\mathrm{TX}},k}^{(0)}$ (light blue arrows; step 0). These messages are sent only once and they are used as prior information to compute the outgoing messages to all connected factor nodes (red arrows; step 1.1). From the factor nodes $q^{(l)}$ and $v^{(j)}$ of legacy and new PFs, the outgoing messages to the DA layer (light green arrows; step 1.2) are computed. In the *data association layer*,

$N_{\rm DA}$ iterations are performed (not indicated). Then, the outgoing messages towards the *data fusion layer* (magenta arrows; step 2) are computed. We use only legacy features to update the UE states. Hence only messages from $q^{(l)}$ are sent towards the UE states (orange arrows; step 3), but no messages from $v^{(j)}$. After messages from the $q^{(l)}$ factor nodes have been sent to the UE states, one data fusion iteration is completed. Note that for each data fusion iteration, there are $N_{\rm DA}$ data association iterations. After $N_{\rm DF}$ iterations in the data fusion layer, the outgoing messages to the prediction nodes of the next time step (dark blue arrows; step 4) are calculated. These messages are at the same time the beliefs used for joint detection and estimation as described in Section IV-A.

So far, we have presented how the messages in COMPAS are calculated. Most of the messages that leave factor nodes cannot be solved in a closed form due to the integrals that are contained. We use Monte Carlo integration and importance sampling to approximate the continuous messages by particles (samples with associated weights). If the incoming messages to a factor node are given as a set of particles, the particles of all messages can be stacked together [17]. In this way, only a single higher dimensional Monte Carlo integration has to be performed in order to compute the outgoing message. This "stacking operation" results in a linear scaling of the computational complexity in the number of particles $N_{\rm s}$. However, due to the *curse of dimensionality* [65], the accuracy of this single higher dimensional Monte Carlo integration may be poor. For a good tradeoff between inference accuracy and computational complexity, we found it particularly useful to only stack UE state particles and perform an additional Monte Carlo integration over the PF state, i.e., for every UE state particle, we carry out a Monte Carlo integral using the PF particles.

The computational complexity of the resulting Monte Carlo-based computations scales quadratically in $N_{\rm s}$. Furthermore, $N_{\rm s}$ is constant in the number of PF states $L_k + M_k$ and the overall complexity scales only quadratically in the number of PF states $L_k + M_k$. A major reason for this favorable scalability is the integration of a BP-based probabilistic DA scheme involving both feature-oriented and measurement-oriented association variables [53], [61], [62] in the overall BP-based algorithm.

V. Numerical Evaluation of COMPAS

The numerical analysis of the proposed method consists of two parts. In part A, an analysis of the data fusion layer is considered in a static scenario. This analysis is performed in order to compare the estimation accuracy with the fundamental limits embodied by the Cramér-Rao lower bounds (CRLBs). For this analysis to be feasible, it is assumed that the association of features with measurements is known and that there are no missed detections and clutter measurements. Moreover, it is assumed that the number of features in the propagation environment is known. Part B of the numerical analysis is dedicated to the dynamic scenario with data association uncertainty, clutter measurements, and missed detections. In the dynamic scenario, we consider vehicle localization in an urban canyon to demonstrate the capabilities of COMPAS to determine the UE states and infer the propagation environment.

The following simulation parameters are used in both scenarios. The measurement noise is zero-mean additive white Gaussian noise with standard deviations $\sigma_{{\rm RX},k} = \sigma^{(j)}_{{\rm RX},k} = \sigma_{{\rm TX},k} = \sigma^{(j)}_{{\rm TX},k} = 1$ deg and $c\sigma_{\tau_k} = c\sigma^{(j)}_{\tau_k} = 0.2$ m, $\forall j,k$. Furthermore,

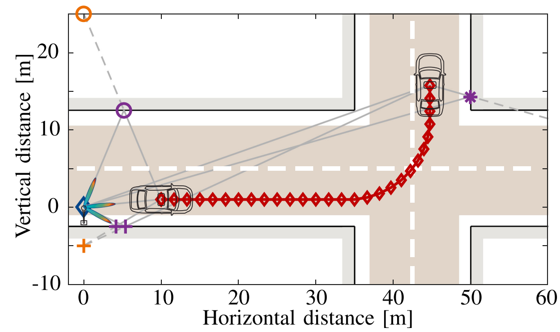

Fig. 7. Trajectory of the UE. The UE (vehicle) takes a left turn on an urban corner. The walls of the buildings (black lines) reflect the transmitted signals from the BS (blue diamond) towards the UE. The VAs (orange markers), reflection points (magenta markers), and paths (gray lines) at the start and end of the trajectory are shown. The VA with the '*'-marker is not displayed.

at time $k = 1$, the prior PDFs $f(\boldsymbol{p}_1)$, $f(\alpha_1)$, and $f(\epsilon_1)$ are Gaussian with standard deviations $\sigma_{p_{\rm x}} = \sigma_{p_{\rm y}} = 5$ m, $\sigma_\alpha = 10$ deg, and $c\sigma_\epsilon = 5$ m. The mean values of each Gaussian prior PDF are treated as hyper-parameters whose values are drawn randomly. For instance, the prior mean m_α of the orientation is drawn as $m_\alpha \sim \mathcal{N}(\alpha, \sigma^2_\alpha)$ where α is the true orientation and $\mathcal{N}(\alpha, \sigma^2_\alpha)$ denotes the Gaussian distribution with mean α and variance σ^2_α. The BS and the relevant[7] VAs are located at $\boldsymbol{q} = [0,0]^{\rm T}$ m, $\boldsymbol{p}^{(1)}_{\rm VA} = [0,-5]^{\rm T}$ m, $\boldsymbol{p}^{(2)}_{\rm VA} = [0,25]^{\rm T}$ m, and $\boldsymbol{p}^{(3)}_{\rm VA} = [100,0]^{\rm T}$ m. We performed $N_{\rm MC} = 100$ simulation runs.

A. Static Scenario

The estimation performance of the proposed data fusion layer will be investigated in this subsection using an exemplary geometry. Particularly, the start point $\boldsymbol{p}_1 = [10,1]^{\rm T}$ m (leftmost red diamond in Fig. 7) of the trajectory depicted in Fig. 7 will be considered. The orientation in that point is $\alpha_1 = 0$ deg and the clock offset between the BS and UE is $c\epsilon_1 = 4.5$ m. We assume that one of the present NLOS paths is received and the corresponding reflector is located at $\boldsymbol{s}^{(2)}_1 = [5.208, 12.5]^{\rm T}$ m (magenta circle in Fig. 7). The root-mean-square errors (RMSEs) on the UE position, orientation, and clock offset as well as the reflector position achieved by the proposed data fusion layer will be compared to the CRLBs derived in [51]. We use $N_{\rm s} = 250$ or $N_{\rm s} = 2000$ particles.

Fig. 8 depicts the RMSEs versus the number $N_{\rm DF}$ of iterations in the data fusion layer. The RMSEs in iteration $N_{\rm DF} = 0$ correspond to the standard deviations of the priors. Since no prior information is assumed on the reflector, there is no marker in the bottom-most plot. The results in Fig. 8 demonstrate that the CRLBs of all estimation parameters can be attained by using $N_{\rm s} = 2000$ particles. The number $N_{\rm DF}$ of iterations necessary to reach the bounds is different for each estimation parameter. For all estimation parameters, convergence is roughly achieved if $N_{\rm DF} > 10$. Different geometric constellations yield similar results in terms of the estimation accuracy. Yet, the number of required iterations to achieve convergence is geometry-dependent. Moreover, it is worth mentioning that the achieved RMSEs are often slightly higher than the CRLBs, if more than one reflector is present.

[7]By relevant we mean those VAs that correspond to walls which are illuminated at least once during the course of the trajectories.

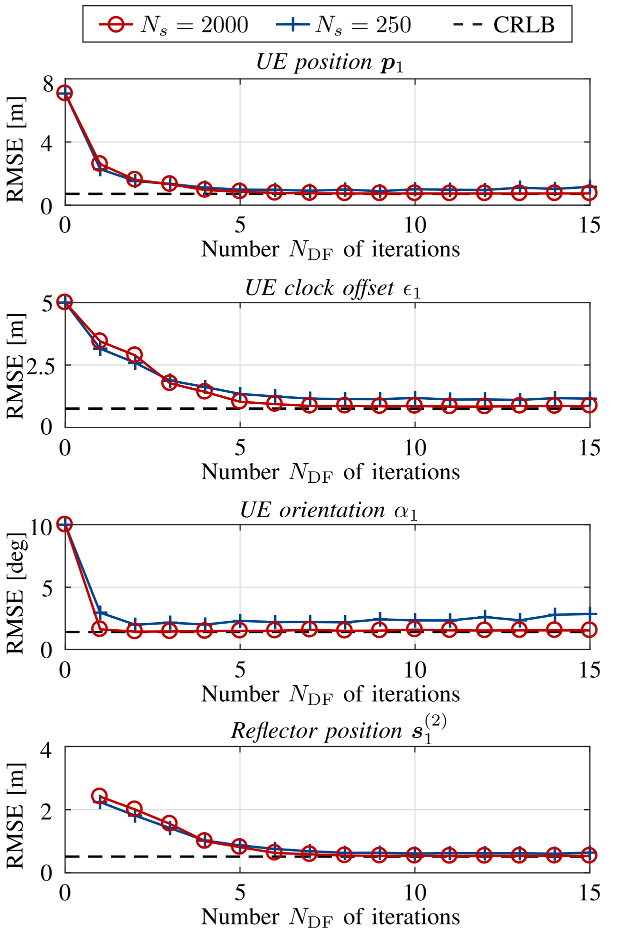

Fig. 8. Achieved estimation accuracy and the attainable accuracy versus the number N_{DF} of iterations. The proposed data fusion layer approaches the CRLBs for a sufficiently large number of iterations and particles.

B. Dynamic Scenario

We consider a vehicle that moves along the trajectory depicted in the Fig. 7 as UE. In our dynamic scenario, inferring the propagation environment is complicated by data association uncertainty, clutter measurements, and missed detections. In this subsection, four different analyses are conducted. First, we compare COMPAS to its "genie-aided" version that can perfectly identify clutter measurements and perfectly associate measurements to PFs. Next, we study the dependence of the state estimation and mapping capabilities on different system parameters, namely, varying detection probability P_{d}, clutter intensity λ_{c}, and LOS probability P_{LOS}.

The following parameters are considered. The probability of detection is constant, i.e., $P_{\mathrm{d}}(\breve{\boldsymbol{p}}_{\mathrm{VA},k}, \mathbf{p}_k, \alpha_k) = P_{\mathrm{d}}$. Clutter measurements of angles and delays are uniformly distributed on the intervals $[0, 360)$ deg and $[0, 100]$ m. The intensity function of newly detected features is constant in time k, i.e., $\lambda_{\mathrm{n},k}(\breve{\boldsymbol{p}}_{\mathrm{VA},k}) = \lambda_{\mathrm{n}}(\breve{\boldsymbol{p}}_{\mathrm{VA},k})$ and uniformly distributed on the area shown in Fig. 7. The mean number of newly detected features is $m_{\mathrm{n}} = \int \lambda_{\mathrm{n}}(\breve{\boldsymbol{p}}_{\mathrm{VA},k})\mathrm{d}\breve{\boldsymbol{p}}_{\mathrm{VA},k} = 0.01$. The survival probability and birth intensity function are set to $P_{\mathrm{s}}(\boldsymbol{p}_{\mathrm{VA},k}^{(l)}) = P_{\mathrm{s}} = 0.999$ and $\lambda_{\mathrm{b}}(\breve{\boldsymbol{p}}_{\mathrm{VA},k}) = 0$, respectively. The UE has a speed of $v = 10$ m/s and its turn rate w depends on its location (see Fig. 7). At each time step k, the UE obtains a noisy observation of its speed and turn-rate. This observation is corrupted by zero-mean additive Gaussian noise with standard deviations of $\sigma_v = 0.1$ m/s as well as $\sigma_w = 0.1$ deg/s and used in the state transition function of the UE. The duration of a time step is 200 ms. A PF with state $\mathsf{x}_k^{(l)} = [\mathbf{p}_{\mathrm{VA},k}^{(l)T}\ \mathsf{r}_k^{(l)T}]$ is declared to exist if $\mathbb{P}(\mathsf{r}_k^{(l)} = 1) > P_{\mathrm{ex}} = 0.5$. We prune a PF l if $\mathbb{P}(\mathsf{r}_k^{(l)} = 1) \leq 10^{-4}$. Furthermore, we set $N_{\mathrm{DF}} = 5$, $N_{\mathrm{DA}} = 10^4$, and $N_{\mathrm{s}} = 2000$ particles.

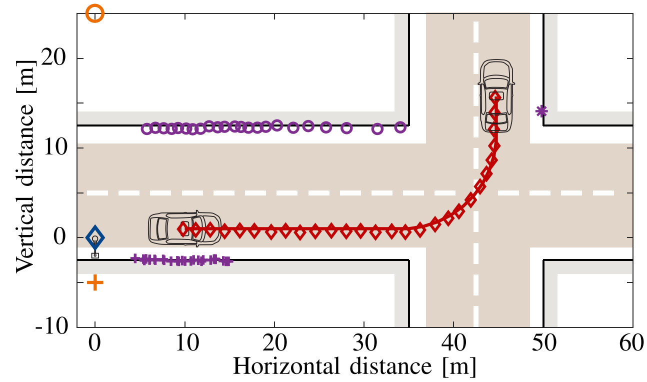

Fig. 9. Example of an estimated trajectory of the UE and the points of reflection. Squares, circles, and asterisks visualize the points of reflection at different time instances if VAs exceed the existence threshold. Diamonds depict the estimated locations of the UE, and the solid red line displays the ground truth trajectory.

The results of a typical realization of the estimated trajectories of the reflections points (obtained from the VA and UE positions via (4)) and UE positions are depicted in Fig. 9. Every marker visualizes an estimate. Comparing Fig. 9 with Fig. 7, we can see that the estimated trajectory closely follows the true trajectory and that the reflection points reside on the surfaces of the reflecting walls. The Figs. 10–13 depict the numerical results of the four considered analyses. All figures contain five subplots, which depict different metrics over the course of the trajectory of the UE. The first three subplots depict the RMSEs of the UE states. The fourth and fifth subplots depict the cardinality of VAs that are declared to exist and the sum of their errors measured under the Euclidean norm, respectively. The fourth subplot also shows the ground truth cardinality of existing VAs.

1) Benchmark Comparison: Fig. 10 shows the comparison of COMPAS with its genie-aided version. The probability of detection and the mean number of clutter measurements are $P_{\mathrm{d}} = 0.9$ and $m_{\mathrm{c}} = 0.1$, respectively. It can be observed that the UE state estimation accuracies of COMPAS and its genie-aided version are almost identical. In terms of mapping capabilities, the genie-aided version of COMPAS shows a faster adaption to changes in the number of VAs and a slightly lower cardinality error compared to COMPAS. Yet, the mapping performance is similar in the case of low clutter ($m_{\mathrm{c}} = 0.1$).

2) Clutter Intensity: Fig. 11 studies the impact of the clutter intensity on UE state estimation accuracy and mapping capabilities of COMPAS. For this analysis, mean numbers of clutter measurements $m_{\mathrm{c}} = 0.1$ and $m_{\mathrm{c}} = 4$ are considered. The detection probability is set to $P_{\mathrm{d}} = 0.9$. We can see that COMPAS is resilient to clutter since the UE state estimation accuracy is not greatly affected by a change of the clutter intensity. Moreover, we can observe that the number of VAs that are declared to exist almost attains the ground truth after some time steps. In the strong clutter ($m_{\mathrm{c}} = 4$) case, this process takes

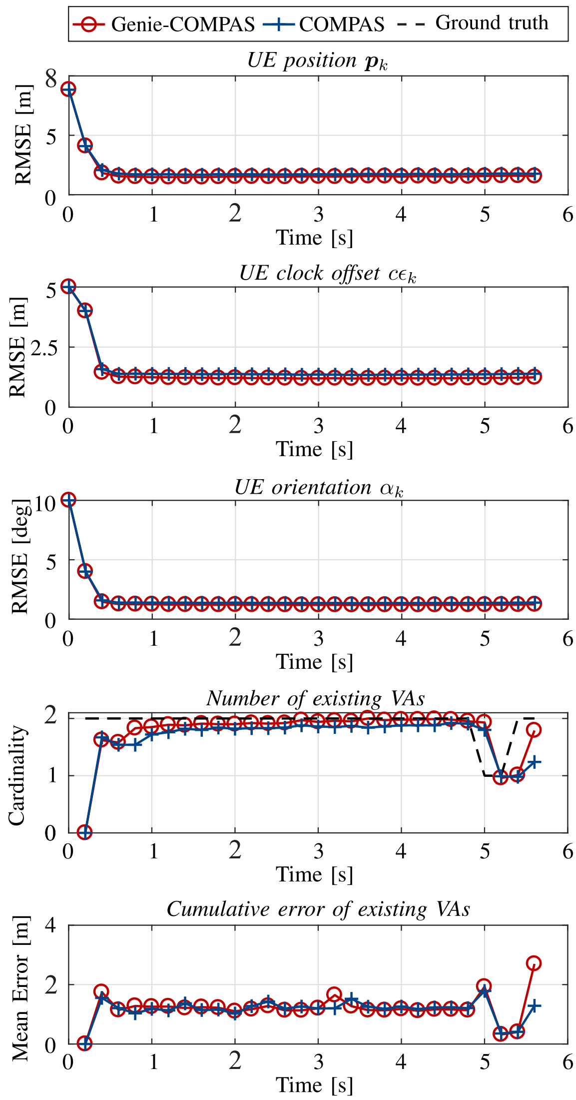

Fig. 10. Average UE and VA metrics over the course of the trajectory. The UE state estimation and mapping performance of COMPAS is only moderately affected by data association uncertainty and clutter.

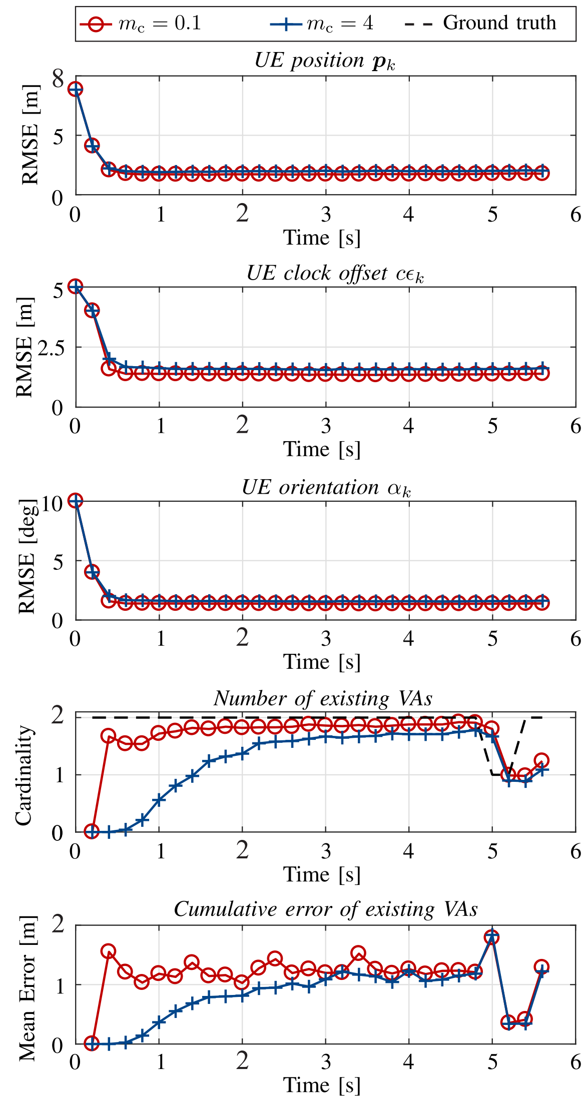

Fig. 11. Clutter intensity. The presence of clutter does not affect the UE performance metrics considerably.

somewhat longer. Finally, we can see from the fifth subplot that existing VAs can be localized accurately. Bear in mind that the metric in the fifth subplot considers solely the errors of VAs that are declared to exist, i.e. the cumulative error is zero if no VAs is declared to exist. The localization accuracy of VAs in the presence of strong clutter is not higher than those in weak clutter, but fewer VAs are declared to exist and hence fewer errors are summed up.

3) Detection Probability: The numerical results in the context of different detection probabilities are depicted in Fig. 12. In this analysis, we consider a mean number of clutter measurements of $m_{\mathrm{c}} = 0.1$ as well as detection probabilities $P_{\mathrm{d}} = 0.95$ and $P_{\mathrm{d}} = 0.8$. We observe that the estimation accuracy of the UE states degrades only slightly if the detection probability is reduced from $P_{\mathrm{d}} = 0.95$ to $P_{\mathrm{d}} = 0.8$. However, there is an increase in the average cardinality error due to the decreased detection probability. While the number of VAs is almost correctly determined after a few time steps in the case of $P_{\mathrm{d}} = 0.95$, more frequent missed detections in the case of $P_{\mathrm{d}} = 0.8$ result in a lower number of VAs that are declared to exist than actually existing VAs.

4) LOS Probability: In this numerical analysis, the existence of a LOS path is modeled as a Bernoulli random variable with LOS probability P_{LOS} that is statistically independent across different time steps. Fig. 13 depicts the results for different LOS probabilities P_{LOS}. The detection probability and mean number clutter measurements are chosen as $P_{\mathrm{d}} = 0.95$ and $m_{\mathrm{c}} = 0.1$, respectively. It can be observed that the UE estimation accuracy is not affect by the the lower LOS probability since the information from NLOS paths and well-localized VAs allows for precise UE state estimation even in the absence of the LOS. However, we can see that the VA estimation accuracy is slightly lower compared to the case with high LOS probability.

VI. Conclusion

Situational-aware communications leverages knowledge on the locations of UEs and their environments to enhance the performance of data transmission. While such knowledge is

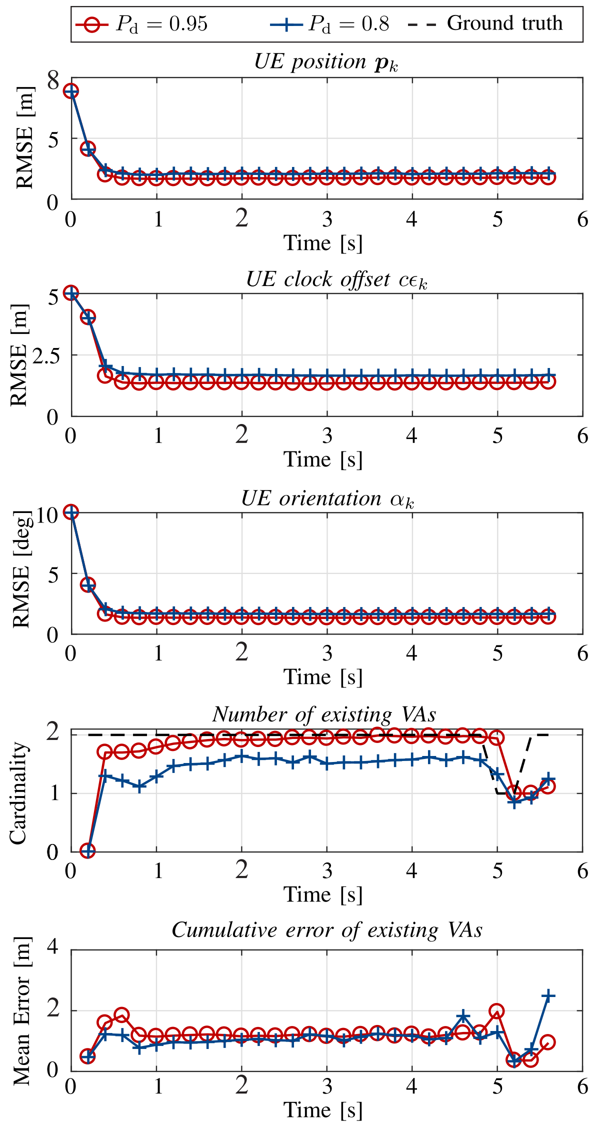

Fig. 12. Detection probability. High detection probability allows for cardinality errors in the number of VAs.

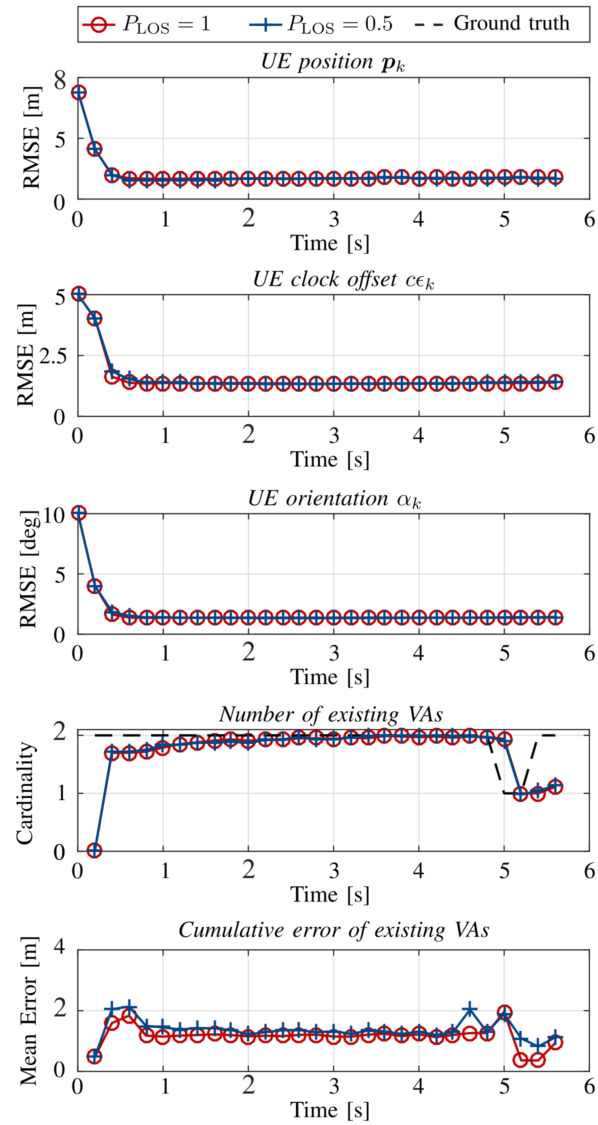

Fig. 13. LOS probability. The absence of the LOS path does not affect the inference performance significantly.

typically unavailable in current mobile radio systems, future mmWave mMIMO communication technology will make it possible to obtain information on locations of UEs and features in their propagation environments based on the received radio signals. We presented COMPAS, a robust and scalable inference engine that infers the UE states (position, orientation, and clock offset) as well as a map of the reflecting surfaces that describe the propagation environment. COMPAS embodies a novel way of discovering the location of a UE and its surrounding, which builds the foundation for situational-aware communication systems. Simulation results demonstrated that COMPAS can approach performance bounds and is resilient to missed detections and clutter.

Appendix A
Derivation of the Joint Posterior Distribution

Let us first introduce the short notation for the joint UE state as $\mathbf{u}_k \triangleq [\mathbf{p}_k^{\mathrm{T}}\ \alpha_k\ \varepsilon_k]^{\mathrm{T}}$. Now, we develop the conditional PDF of $\mathbf{z}_k, \mathbf{z}_k^{(0)}, \mathbf{a}_k, \mathbf{b}_k, \mathsf{M}_k, \mathbf{x}_k$, and $\mathbf{u}_k$, given $\underline{\mathbf{x}}_{k-1}$ and u_{k-1}. This PDF is obtained as

$$\begin{aligned} &f\big(\boldsymbol{z}_k, \boldsymbol{z}_k^{(0)}, \boldsymbol{a}_k, \boldsymbol{b}_k, M_k, \boldsymbol{x}_k, \boldsymbol{u}_k | \boldsymbol{x}_{k-1}, \boldsymbol{u}_{k-1}\big) \\ &\quad = f\big(\boldsymbol{z}_k, \boldsymbol{z}_k^{(0)}, \boldsymbol{a}_k, \boldsymbol{b}_k, M_k, \overline{\boldsymbol{x}}_k | \underline{\boldsymbol{x}}_k, \boldsymbol{u}_k, \boldsymbol{x}_{k-1}, \boldsymbol{u}_{k-1}\big) \\ &\qquad \times f\big(\underline{\boldsymbol{x}}_k, \boldsymbol{u}_k | \boldsymbol{x}_{k-1}, \boldsymbol{u}_{k-1}\big) \\ &\quad = f\big(\boldsymbol{z}_k, \boldsymbol{z}_k^{(0)}, \boldsymbol{a}_k, \boldsymbol{b}_k, M_k, \overline{\boldsymbol{x}}_k | \underline{\boldsymbol{x}}_k, \boldsymbol{u}_k\big) f\big(\underline{\boldsymbol{x}}_k, \boldsymbol{u}_k | \boldsymbol{x}_{k-1}, \boldsymbol{u}_{k-1}\big). \end{aligned} \tag{28}$$

Here we used the assumption (cf. [44], [53]) that given the current VA states $\underline{\mathbf{x}}_k$ and the current UE state $\mathbf{u}_k$, the measurements $\mathbf{z}_k$ and $\mathbf{z}_k^{(0)}$, the number of NLOS measurements M_k, as well as the association variables $\mathbf{a}_k$ and $\mathbf{b}_k$ are statistically independent of $\mathbf{x}_{k-1}$, and $\mathbf{u}_{k-1}$. Note that for $k = 1$, $f(\underline{\boldsymbol{x}}_1, \boldsymbol{u}_1 | \boldsymbol{x}_0, \boldsymbol{u}_0) \triangleq f(\boldsymbol{u}_1)$.

Next, we develop the conditional PDF of $\mathsf{z}_k, \mathsf{z}_k^{(0)}, \mathsf{a}_k, \mathsf{b}_k, \mathsf{M}_k$, and $\overline{\mathsf{x}}_k$ given $\underline{\mathsf{x}}_k$ and u_k. We obtain

$$\begin{aligned} &f\big(\boldsymbol{z}_k, \boldsymbol{z}_k^{(0)}, \boldsymbol{a}_k, \boldsymbol{b}_k, M_k, \overline{\boldsymbol{x}}_k | \underline{\boldsymbol{x}}_k, \boldsymbol{u}_k\big) \\ &\quad = f\big(\boldsymbol{z}_k^{(0)} | \boldsymbol{z}_k, \boldsymbol{a}_k, \boldsymbol{b}_k, M_k, \boldsymbol{x}_k, \boldsymbol{u}_k\big) \\ &\qquad \times f\big(\boldsymbol{z}_k, \boldsymbol{a}_k, \boldsymbol{b}_k, M_k, \overline{\boldsymbol{x}}_k | \underline{\boldsymbol{x}}_k, \boldsymbol{u}_k\big) \\ &\quad = f\big(\boldsymbol{z}_k^{(0)} | \boldsymbol{u}_k\big) f\big(\boldsymbol{z}_k, \boldsymbol{a}_k, \boldsymbol{b}_k, M_k, \overline{\boldsymbol{x}}_k | \underline{\boldsymbol{x}}_k, \boldsymbol{u}_k\big), \end{aligned} \tag{29}$$

where we assumed that given u_k, the LOS measurements $\mathsf{z}_k^{(0)}$ are statistically independent of the NLOS measurements z_k and their number M_k, the VA states x_k, as well as the association variables a_k and b_k.

By using the same assumptions and following the same steps as in [44], [53], the PDF of z_k, a_k, b_k, M_k, and $\overline{\mathsf{x}}_k$ conditioned on $\underline{\mathsf{x}}_k$, u_k is obtained as

$$\begin{aligned} &f(\boldsymbol{z}_k, \boldsymbol{a}_k, \boldsymbol{b}_k, M_k, \overline{\boldsymbol{x}}_k | \underline{\boldsymbol{x}}_k, \boldsymbol{u}_k) = C(\boldsymbol{z}_k)\, \Psi(\boldsymbol{a}_k, \boldsymbol{b}_k) \\ &\quad \times \left(\prod_{l=1}^{L_k} q\left(\underline{\boldsymbol{p}}_{\mathrm{VA},k}^{(l)}, \underline{r}_k^{(l)}, \boldsymbol{p}_k, \alpha_k, \epsilon_k, a_k^{(l)}; \boldsymbol{z}_k \right) \right) \\ &\quad \times \prod_{j=1}^{M_k} v\big(\overline{\boldsymbol{p}}_{\mathrm{VA},k}^{(j)}, \overline{r}_k^{(j)}, \boldsymbol{p}_k, \alpha_k, \epsilon_k, b_k^{(j)}; \boldsymbol{z}_k^{(j)}\big). \end{aligned} \tag{30}$$

Here, $C(\boldsymbol{z}_k)$ is a normalization factor that depends only on $\boldsymbol{z}_k$ and $q(\underline{\boldsymbol{p}}_{\mathrm{VA},k}^{(l)}, \underline{r}_k^{(l)}, \boldsymbol{p}_k, \alpha_k, \epsilon_k, a_k^{(l)}; \boldsymbol{z}_k)$ is defined in (14) and (15). Furthermore, $v(\overline{\boldsymbol{p}}_{\mathrm{VA},k}^{(j)}, \overline{r}_k^{(j)}, \boldsymbol{p}_k, \alpha_k, \epsilon_k, b_k^{(j)}; \boldsymbol{z}_k^{(j)})$ is defined in (16) and (17). For $k = 1$, an expression for $f(\boldsymbol{z}_1, \boldsymbol{a}_1, \boldsymbol{b}_1, m_1, \overline{\boldsymbol{x}}_1 | \underline{\boldsymbol{x}}_0, \boldsymbol{u}_0) \triangleq f(\boldsymbol{z}_1, \boldsymbol{b}_1, m_1, \overline{\boldsymbol{x}}_1)$ is obtained by replacing in (30) the product involving L_k as well as the factor $\Psi(\boldsymbol{a}_k, \boldsymbol{b}_k)$ by one.

Next, we use the chain rule as well as the assumption [44], [53] that at time k, given VA states x_{k-1}, and UE state u_{k-1}, the current measurements $\mathsf{z}_k^{(0)}$, z_k and their number M_k as well as variables a_k, b_k, x_k, and u_k are conditionally independent of all the past measurements $\mathsf{z}_{k-1}^{(0)}$, z_{k-1} and their number M_{k-1} as well as past association vectors a_{k-1} and b_{k-1}. The unconditional joint PDF for all times up to K can then be obtained as

$$\begin{aligned} &f(\boldsymbol{z}_{1:K}, \boldsymbol{M}_{1:K}, \boldsymbol{u}_{1:K}, \boldsymbol{x}_{1:K}, \boldsymbol{a}_{1:K}, \boldsymbol{b}_{1:K}) \\ &\quad = \prod_{k=1}^{K} f\big(\boldsymbol{z}_k, \boldsymbol{z}_k^{(0)}, \boldsymbol{a}_k, \boldsymbol{b}_k, M_k, \boldsymbol{x}_k, \boldsymbol{u}_k | \boldsymbol{x}_{k-1}, \boldsymbol{u}_{k-1}\big). \end{aligned} \tag{31}$$

With $\boldsymbol{z}_{1:k}$ observed and thus fixed, we obtain the following expression for the joint posterior PDF

$$\begin{aligned} &f(\boldsymbol{u}_{1:K}, \boldsymbol{x}_{1:K}, \boldsymbol{a}_{1:K}, \boldsymbol{b}_{1:K} | \boldsymbol{z}_{1:K}) \\ &\quad = f(\boldsymbol{u}_{1:K}, \boldsymbol{x}_{1:K}, \boldsymbol{a}_{1:K}, \boldsymbol{b}_{1:K} | \boldsymbol{z}_{1:K}, \boldsymbol{M}_{1:K}) \\ &\quad \propto f(\boldsymbol{z}_{1:K}, \boldsymbol{M}_{1:K}, \boldsymbol{u}_{1:K}, \boldsymbol{x}_{1:K}, \boldsymbol{a}_{1:K}, \boldsymbol{b}_{1:K}) \\ &\quad = \prod_{k=1}^{K} f\big(\boldsymbol{z}_k, \boldsymbol{z}_k^{(0)}, \boldsymbol{a}_k, \boldsymbol{b}_k, M_k, \boldsymbol{x}_k, \boldsymbol{u}_k | \boldsymbol{x}_{k-1}, \boldsymbol{u}_{k-1}\big) \end{aligned}$$

where (31) was used.

Next, using (28) and subsequently (29) and (30), we obtain further

$$\begin{aligned} &f(\boldsymbol{u}_{1:K}, \boldsymbol{x}_{1:K}, \boldsymbol{a}_{1:K}, \boldsymbol{b}_{1:K} | \boldsymbol{z}_{1:K}) \\ &\quad \propto \prod_{k=1}^{K} f\big(\underline{\boldsymbol{x}}_k, \boldsymbol{u}_k | \boldsymbol{x}_{k-1}, \boldsymbol{u}_{k-1}\big) f\big(\boldsymbol{z}_k^{(0)} | \boldsymbol{u}_k\big) \\ &\qquad \times \Psi(\boldsymbol{a}_k, \boldsymbol{b}_k) \left(\prod_{l=1}^{L_k} q\big(\underline{\boldsymbol{p}}_{\mathrm{VA},k}^{(l)}, \underline{r}_k^{(l)}, \boldsymbol{p}_k, \alpha_k, \epsilon_k, a_k^{(l)}; \boldsymbol{z}_k\big) \right) \\ &\qquad \times \prod_{j=1}^{M_k} v\big(\overline{\boldsymbol{p}}_{\mathrm{VA},k}^{(j)}, \overline{r}_k^{(j)}, \boldsymbol{p}_k, \alpha_k, \epsilon_k, b_k^{(j)}; \boldsymbol{z}_k^{(j)}\big). \end{aligned}$$

Finally, recalling that $\mathsf{u}_k = [\mathsf{p}_k^{\mathrm{T}}\ \alpha_k\ \epsilon_k]^{\mathrm{T}}$ and inserting (5), (7), and (11), yields the final expression in (13).

Acknowledgment

The authors would like to thank A. Conti, F. Jiang, Z. Liu, T. Peng, A. Saucan, and Z. Yu for their helpful suggestions and careful reading of the manuscript.

References

[1] M. Z. Win *et al.*, "Network localization and navigation via cooperation," *IEEE Commun. Mag.*, vol. 49, no. 5, pp. 56–62, May 2011.

[2] M. Z. Win, F. Meyer, Z. Liu, W. Dai, S. Bartoletti, and A. Conti, "Efficient multi-sensor localization for the Internet-of-Things," *IEEE Signal Process. Mag.*, vol. 35, no. 5, pp. 153–167, Sep. 2018.

[3] A. T. Ihler, J. W. Fisher III, R. L. Moses, and A. S. Willsky, "Nonparametric belief propagation for self-localization of sensor networks," *IEEE J. Sel. Areas Commun.*, vol. 23, no. 4, pp. 809–819, Apr. 2005.

[4] S. Gezici *et al.*, "Localization via ultra-wideband radios: A look at positioning aspects for future sensor networks," *IEEE Signal Process. Mag.*, vol. 22, no. 4, pp. 70–84, Jul. 2005.

[5] M. Z. Win, Y. Shen, and W. Dai, "A theoretical foundation of network localization and navigation," *Proc. IEEE*, vol. 106, no. 7, pp. 1136–1165, Jul. 2018, special issue on *Foundations and Trends in Localization Technologies*.

[6] Y. Shen and M. Z. Win, "Fundamental limits of wideband localization – Part I: A general framework," *IEEE Trans. Inf. Theory*, vol. 56, no. 10, pp. 4956–4980, Oct. 2010.

[7] U. A. Khan, S. Kar, and J. M. F. Moura, "DILAND: An algorithm for distributed sensor localization with noisy distance measurements," *IEEE Trans. Signal Process.*, vol. 58, no. 3, pp. 1940–1947, Mar. 2010.

[8] U. Khan, S. Kar, and J. Moura, "Linear theory for self-localization: Convexity, barycentric coordinates, and Cayley-Menger determinants," *IEEE Access*, vol. 3, pp. 1326–1339, Aug. 2015.

[9] S. Safavi, U. A. Khan, S. Kar, and J. M. F. Moura, "Distributed localization: A linear theory," *Proc. IEEE*, vol. 106, no. 7, pp. 1204–1223, Jul. 2018.

[10] M. Z. Win, W. Dai, Y. Shen, G. Chrisikos, and H. V. Poor, "Network operation strategies for efficient localization and navigation," *Proc. IEEE*, vol. 106, no. 7, pp. 1224–1254, Jul. 2018, special issue on *Foundations and Trends in Localization Technologies*.

[11] R. Niu, A. Vempaty, and P. K. Varshney, "Received signal strength based localization in wireless sensor networks," *Proc. IEEE*, vol. 106, no. 6, pp. 1166–1182, Jun. 2018.

[12] E. Maşazade, R. Niu, P. K. Varshney, and M. Keskinoz, "Energy aware iterative source localization for wireless sensor networks," *IEEE Trans. Signal Process.*, vol. 58, no. 9, pp. 4824–4835, Jun. 2010.

[13] R. Niu, R. S. Blum, P. K. Varshney, and A. L. Drozd, "Target localization and tracking in noncoherent multiple-input multiple-output radar systems," *IEEE Trans. Aerosp. Electron. Syst.*, vol. 48, no. 2, pp. 1466–1489, Apr. 2012.

[14] S. Bartoletti, W. Dai, A. Conti, and M. Z. Win, "A mathematical model for wideband ranging," *IEEE J. Sel. Topics Signal Process.*, vol. 9, no. 2, pp. 216–228, Mar. 2015.

[15] M. Z. Win, S. Bartoletti, W. Dai, and A. Conti, "Wideband ranging system," U.S. Utility Patent Application US 2018/0 356 494 A1, Dec. 13, 2018.

[16] K. Plarre and P. R. Kumar, "Tracking objects with networked scattered directional sensors," *EURASIP J. Adv. Signal Process.*, vol. 2008, Jan. 2008, Art. no. 74.

[17] F. Meyer, O. Hlinka, H. Wymeersch, E. Riegler, and F. Hlawatsch, "Distributed localization and tracking of mobile networks including noncooperative objects," *IEEE Trans. Signal Inf. Process. Netw.*, vol. 2, no. 1, pp. 57–71, Mar. 2016.

[18] S. Mazuelas, A. Conti, J. C. Allen, and M. Z. Win, "Soft range information for network localization," *IEEE Trans. Signal Process.*, vol. 66, no. 12, pp. 3155–3168, Jun. 2018.

[19] S. Aditya, A. F. Molisch, and H. M. Behairy, "A survey on the impact of multipath on wideband time-of-arrival based localization," *Proc. IEEE*, vol. 106, no. 7, pp. 1183–1203, Jul. 2018.

[20] B. Teague, Z. Liu, F. Meyer, and M. Z. Win, "Peregrine: 3-D network localization and navigation," in *Proc. IEEE Latin-Amer. Conf. Commun.*, Guatemala City, Guatemala, Nov. 2017, pp. 1–6.

[21] F. Zabini and A. Conti, "Inhomogeneous Poisson sampling of finite-energy signals with uncertainties in $\mathbb{R}^d$," *IEEE Trans. Signal Process.*, vol. 64, no. 18, pp. 4679–4694, Sep. 2016.

[22] E. Arias-de-Reyna, P. Closas, D. Dardari, and P. M. Djuric, "Crowd-based learning of spatial fields for the Internet of Things: From harvesting of data to inference," *IEEE Signal Process. Mag.*, vol. 35, no. 5, pp. 130–139, Sep. 2018.

[23] N. Decarli, A. Guerra, A. Conti, R. D'Errico, A. Sibille, and D. Dardari, "Non-regenerative relaying for network localization," *IEEE Trans. Wireless Commun.*, vol. 13, no. 1, pp. 174–185, Jan. 2014.

[24] A. Conti, M. Guerra, D. Dardari, N. Decarli, and M. Z. Win, "Network experimentation for cooperative localization," *IEEE J. Sel. Areas Commun.*, vol. 30, no. 2, pp. 467–475, Feb. 2012.

[25] Z. Liu, W. Dai, and M. Z. Win, "Mercury: An infrastructure-free system for network localization and navigation," *IEEE Trans. Mobile Comput.*, vol. 17, no. 5, pp. 1119–1133, May 2018.

[26] R. D. Taranto, S. Muppirisetty, R. Raulefs, D. T. Slock, T. Svensson, and H. Wymeersch, "Location-aware communications for 5G networks: How location information can improve scalability, latency, and robustness of 5G," *IEEE Signal Process. Mag.*, vol. 31, no. 6, pp. 102–112, Nov. 2014.

[27] J.-C. Aviles and A. Kouki, "Position-aided mm-Wave beam training under NLOS conditions," *IEEE Access*, vol. 4, pp. 8703–8714, 2016.

[28] R. Sachan, T.-J. Choi, and C.-W. Ahn, "A genetic algorithm with location intelligence method for energy optimization in 5G wireless networks," *Discrete Dyn. Nat. Soc.*, vol. 2016, pp. 1–10, 2016.

[29] E. Leitinger, P. Meissner, C. Rüdisser, G. Dumphart, and K. Witrisal, "Evaluation of position-related information in multipath components for indoor positioning," *IEEE J. Sel. Areas Commun.*, vol. 33, no. 11, pp. 2313–2328, Nov. 2015.

[30] K. Witrisal *et al.*, "High-accuracy localization for assisted living," *IEEE Signal Process. Mag.*, vol. 33, no. 2, pp. 59–70, Mar. 2016.

[31] H. Zhang and S. Y. Tan, "TOA based indoor localization and tracking via single-cluster PHD filtering," in *Proc. GLOBECOM*, Dec. 2017, pp. 1–6.

[32] C. Gentner, T. Jost, W. Wang, S. Zhang, A. Dammann, and U. Fiebig, "Multipath assisted positioning with simultaneous localization and mapping," *IEEE Trans. Wireless Commun.*, vol. 15, no. 9, pp. 6104–6117, Sep. 2016.

[33] M. Ulmschneider, C. Gentner, T. Jost, and A. Dammann, "Association of transmitters in multipath-assisted positioning," in *Proc. IEEE GLOBECOM*, Dec. 2017, pp. 1–7.

[34] M. Ulmschneider, C. Gentner, T. Jost, and A. Dammann, "Rao-Blackwellized Gaussian sum particle filtering for multipath assisted positioning," *J. Elect. Comput. Eng.*, vol. 2018, pp. 1–15, Apr. 2018.

[35] F. Rusek *et al.*, "Scaling up MIMO: Opportunities and challenges with very large arrays," *IEEE Signal Process. Mag.*, vol. 30, no. 1, pp. 40–60, Jan. 2013.

[36] E. G. Larsson, O. Edfors, F. Tufvesson, and T. L. Marzetta, "Massive MIMO for next generation wireless systems," *IEEE Commun. Mag.*, vol. 52, no. 2, pp. 186–195, Feb. 2014.

[37] R.-W. Heath, N. González-Prelcic, S. Rangan, W. Roh, and A.-M. Sayeed, "An overview of signal processing techniques for millimeter wave MIMO systems," *IEEE J. Sel. Topics Signal Process.*, vol. 10, no. 3, pp. 436–453, Apr. 2016.

[38] Z. Abu-Shaban, X. Zhou, T. Abhayapala, G. Seco-Granados, and H. Wymeersch, "Error bounds for uplink and downlink 3D localization in 5G millimeter wave systems," *IEEE Trans. Wireless Commun.*, vol. 17, no. 8, pp. 4939–4954, Aug. 2018.

[39] R. Mendrzik, H. Wymeersch, G. Bauch, and Z. Abu-Shaban, "Harnessing NLOS components for position and orientation estimation in 5G millimeter wave MIMO," *IEEE Trans. Wireless Commun.*, vol. 18, no. 1, pp. 93–107, Jan. 2019.

[40] A. Shahmansoori, G.-E. Garcia, G. Destino, G. Seco-Granados, and H. Wymeersch, "Position and orientation estimation through millimeter-wave MIMO in 5G systems," *IEEE Trans. Wireless Commun.*, vol. 17, no. 3, pp. 1822–1835, Mar. 2018.

[41] F. Meyer, B. Etzlinger, Z. Liu, F. Hlawatsch, and M. Z. Win, "A scalable algorithm for network localization and synchronization," *IEEE Internet Things J.*, vol. 5, no. 6, pp. 4714–4727, Dec. 2018.

[42] O. Simeone, U. Spagnolini, Y. Bar-Ness, and S. H. Strogatz, "Distributed synchronization in wireless networks," *IEEE Signal Process. Mag.*, vol. 25, no. 5, pp. 81–97, Sep. 2008.

[43] Y. Wu, Q. Chaudhari, and E. Serpedin, "Clock synchronization of wireless sensor networks," *IEEE Signal Process. Mag.*, vol. 28, no. 1, pp. 124–138, Jan. 2011.

[44] E. Leitinger, F. Meyer, F. Hlawatsch, K. Witrisal, F. Tufvesson, and M. Z. Win, "A belief propagation algorithm for multipath-based SLAM," *IEEE Trans. Wireless Commun.*, vol. 18, no. 11, Nov. 2019.

[45] H. Durrant-Whyte and T. Bailey, "Simultaneous localization and mapping: Part I," *IEEE Signal Process. Mag.*, vol. 13, no. 2, pp. 99–110, Jun. 2006.

[46] C. Cadena *et al.*, "Past, present, and future of simultaneous localization and mapping: Towards the robust-perception age," *IEEE Trans. Robot.*, vol. 32, no. 6, pp. 1309–1332, Dec. 2016.

[47] Y. Shen and M. Z. Win, "On the accuracy of localization systems using wideband antenna arrays," *IEEE Trans. Commun.*, vol. 58, no. 1, pp. 270–280, Jan. 2010.

[48] A. Guerra, F. Guidi, and D. Dardari, "Single-anchor localization and orientation performance limits using massive arrays: MIMO vs. beamforming," *IEEE Trans. Wireless Commun.*, vol. 17, no. 8, pp. 5241–5255, Aug. 2018.

[49] Y. Han, Y. Shen, X.-P. Zhang, M. Z. Win, and H. Meng, "Performance limits and geometric properties of array localization," *IEEE Trans. Inf. Theory*, vol. 62, no. 2, pp. 1054–1075, Feb. 2016.

[50] M. Ruble and İ. Güvenç, "Wireless localization for mmWave networks in urban environments," *EURASIP J. Adv. Signal Process.*, vol. 2018, no. 1, pp. 1–19, Jun. 2018.

[51] H. Wymeersch *et al.*, "5G mm Wave downlink vehicular positioning," in *Proc. IEEE GLOBECOM*, Dec. 2018, pp. 1–7.

[52] R. Mendrzik, H. Wymeersch, and G. Bauch, "Joint localization and mapping through millimeter wave MIMO in 5G systems," in *Proc. IEEE GLOBECOM*, Dec. 2018, pp. 1–6.

[53] F. Meyer *et al.*, "Message passing algorithms for scalable multitarget tracking," *Proc. IEEE*, vol. 106, no. 2, pp. 221–259, Feb. 2018.

[54] H. Deng and A. Sayeed, "Mm-wave MIMO channel modeling and user localization using sparse beamspace signatures," in *Proc. IEEE SPAWC*, Jun. 2014, pp. 130–134.

[55] H. Xie, F. Gao, and S. Jin, "An overview of low-rank channel estimation for massive MIMO systems," *IEEE Access*, vol. 4, pp. 7313–7321, 2016.

[56] C. Chen and W. Wu, "Joint AoD, AoA, and channel estimation for MIMO-OFDM systems," *IEEE Trans. Veh. Technol.*, vol. 67, no. 7, pp. 5806–5820, Jul. 2018.

[57] L. Yang, Y. Zeng, and R. Zhang, "Channel estimation for millimeter-wave MIMO communications with lens antenna arrays," *IEEE Trans. Veh. Technol.*, vol. 67, no. 4, pp. 3239–3251, Apr. 2018.

[58] T. S. Rappaport, G. R. MacCartney, M. K. Samimi, and S. Sun, "Wideband millimeter-wave propagation measurements and channel models for future wireless communication system design," *IEEE Trans. Commun.*, vol. 63, no. 9, pp. 3029–3056, Sep. 2015.

[59] Y. Bar-Shalom, P. K. Willett, and X. Tian, *Tracking and Data Fusion: A Handbook of Algorithms*. Storrs, CT, USA: Yaakov Bar-Shalom, 2011.

[60] G. Soldi, F. Meyer, P. Braca, and F. Hlawatsch, "Self-tuning algorithms for multisensor-multitarget tracking using belief propagation," *IEEE Trans. Signal Process.*, vol. 67, no. 15, pp. 3922–3937, Aug. 2019.

[61] F. Meyer, P. Braca, P. Willett, and F. Hlawatsch, "A scalable algorithm for tracking an unknown number of targets using multiple sensors," *IEEE Trans. Signal Process.*, vol. 65, no. 13, pp. 3478–3493, Jul. 2017.

[62] J. L. Williams and R. Lau, "Approximate evaluation of marginal association probabilities with belief propagation," *IEEE Trans. Aerosp. Electron. Syst.*, vol. 50, no. 4, pp. 2942–2959, Oct. 2014.

[63] F. R. Kschischang, B. J. Frey, and H.-A. Loeliger, "Factor graphs and the sum-product algorithm," *IEEE Trans. Inf. Theory*, vol. 47, no. 2, pp. 498–519, Feb. 2001.

[64] H.-A. Loeliger, "An introduction to factor graphs," *IEEE Signal Process. Mag.*, vol. 21, no. 1, pp. 28–41, Jan. 2004.

[65] F. Daum and J. Huang, "Curse of dimensionality and particle filters," in *Proc. IEEE Aerosp.*, vol. 4, Mar. 2003, pp. 1979–1993.